1 Electromagnetic metamaterials and metasurfaces: historical overview, characterization, and the effect of length scales

Christopher L. Holloway[a], *Edward F. Kuester*[b]
[a]National Institute of Standards and Technology, U.S. Department of Commerce, Boulder, CO, United States, [b]Department of Electrical, Computer, and Energy Engineering, University of Colorado at Boulder, Boulder, CO, United States

1.1 Introduction

The study of electromagnetic (EM) interactions with materials has a long and rich history dating back to Fresnel, Maxwell, Rayleigh, and many others [1–4]. Over these nearly 200 years, EM material development and applications have blossomed dramatically, culminating in the recent developments of metamaterials [5–16]. The prefix "meta" is a Greek preposition meaning (among other things) "beyond". Metamaterials are novel, synthetic materials engineered to achieve unique properties not normally found in nature, i.e., materials beyond those occurring naturally. Metamaterials are often realized by arranging a set of small scatterers in a regular array throughout a region of space (Fig. 1.1), thus obtaining some desirable bulk behavior. Artificial dielectrics were early examples of these engineered materials. However, the term metamaterial is a newer designation that includes, but is not limited to, artificial dielectrics. Nor does the term metamaterial refer to classical periodic structures, such as what are now called photonic bandgap (PBG) structures or frequency-selective surfaces (FSSs). The term metamaterial refers to a material or structure with more exotic properties than artificial dielectrics, but which can still be described by bulk material parameters as natural materials can. One particular class of metamaterial that is being studied extensively consists of the so-called "double-negative" (DNG) materials [17–32] (also known as negative-index materials (NIM), backward-wave (BW) media, or left-handed materials (LHM)). Such materials have the property that their effective permittivity and effective permeability are simultaneously negative in a given frequency band. Another property not normally found in nature that can be achieved with metamaterials is that of near-zero refractive index. In this type of material, either the permittivity or permeability is designed to have its real part close to zero. Materials with unique properties such as these have a wide range of potential applications in electromagnetics at frequencies ranging from the low microwaves to optical, including shielding, low-reflection materials, novel substrates, antennas, electronic switches, devices, "perfect lenses," resonators, and of course cloaking, to name only a few.

Dielectric Metamaterials. https://doi.org/10.1016/B978-0-08-102403-4.00006-2

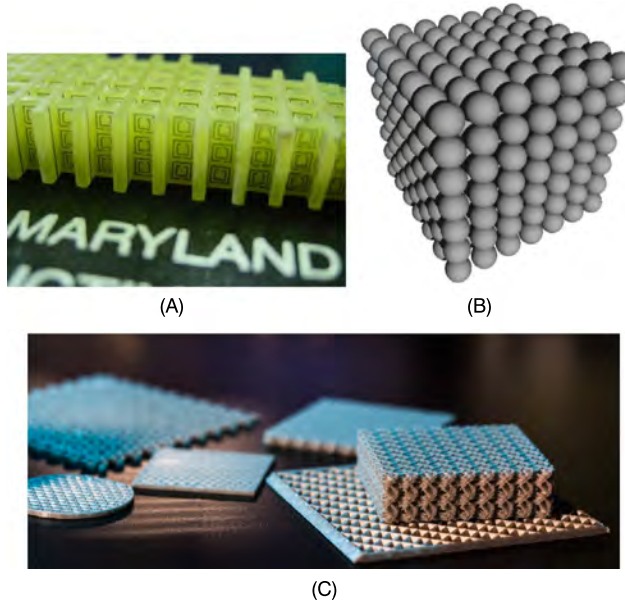

Figure 1.1 Three examples of metamaterials: (A) array of split-rings (Courtesy of Dr. N. Orloff of NIST and Prof. S.M. Anlage of the University of Maryland), (B) array of spherical particles, and (C) array of arbitrarily shaped dielectric inclusions (from Shutterstock, https://www.shutterstock.com/image-photo/example-metamaterials-physics-laboratory-1074505616?src=library).

Initially, the pursuit of cloaking was the "Holy Grail" of these metamaterials and received much attention in the early years of metamaterial research. Cloaking (or the ability to "hide" an object) has appeared throughout the years in popular literature and, depending on your generation, examples include Tolkien's ring, Romulan warships, and Harry Potter's cloak. However, due to physical limitations (no broadband lossless metamaterials are available) cloaking materials have not come to practical fruition. So researchers have turned their attention to other exotic material properties. Properties that are of great interest for a wide range of applications include controllability (that is, a material whose properties can easily be changed over a wide range of frequencies), designs for a very narrow bandwidth, and engineering materials with tailored unnatural permittivities and permeabilities, e.g., materials with near-zero indices.

The concept of metamaterials has been extended to two-dimensional arrays (referred to as metasurfaces) [33,34]; see Figs. 1.1C and 1.2. These types of metastructures have an advantage over three-dimensional metamaterials because they take up less physical space and have the potential for lower losses. Metasurfaces have become a popular alternative to metamaterials. Applications of metasurfaces at frequencies from low microwave to optical have attracted great interest in recent years. These applications in electromagnetics include controllable "smart" surfaces, miniaturized cavity resonators, novel waveguiding structures, angular-independent surfaces, absorbers, biomedical devices, terahertz switches, and fluid-tunable frequency-agile materials, to name only a few.

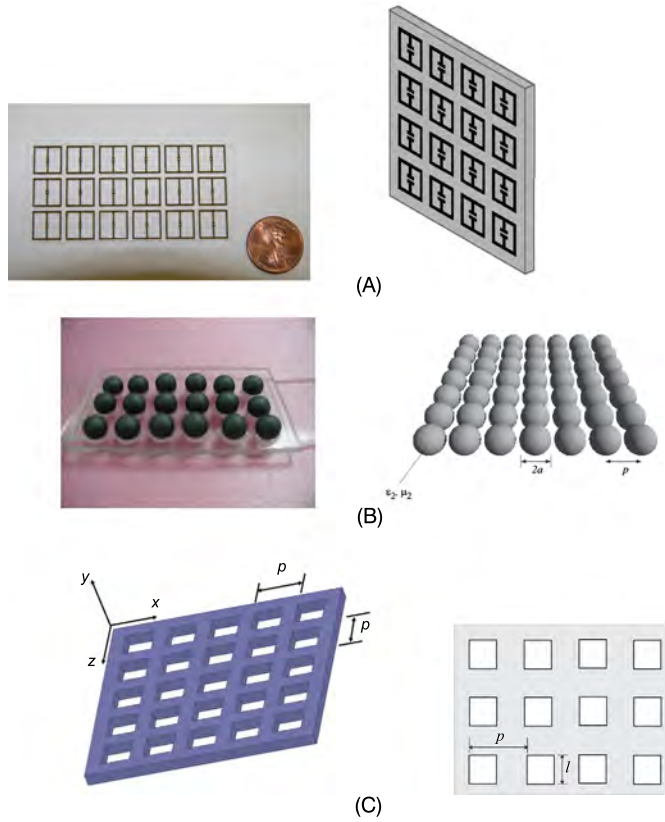

Figure 1.2 Three examples of metasurfaces: (A) array of metallic scatterers (from C.L. Holloway, E.F. Kuester, J.A. Gordon, J. O'Hara, J. Booth, D.R. Smith, An overview of the theory and applications of metasurfaces: the two-dimensional equivalents of metamaterials, IEEE Antennas Propag. Mag. 54 (2) (April 2012) 10–35, © 2012 IEEE), (B) array of magneto-dielectric spherical particles (from C.L. Holloway, E.F. Kuester, J.A. Gordon, J. O'Hara, J. Booth, D.R. Smith, An overview of the theory and applications of metasurfaces: the two-dimensional equivalents of metamaterials, IEEE Antennas Propag. Mag. 54 (2) (April 2012) 10–35, © 2012 IEEE), and (C) array of square apertures (from C.L. Holloway, E.F. Kuester, Generalized sheet transition conditions (GSTCs) for a metascreen, IEEE Trans. Antennas Propag. 66 (5) (2018) 2414–2427, © 2018 IEEE).

The metasurface concept can be extended even further by use of only a linear unit cell, rather than a surface element, as the building block, or even only a single subwavelength resonant element for some desired effect or behavior. In this chapter, we will discuss different aspects of various electromagnetic metastructures. We will provide a historical perspective, a study of the concepts that underly their behavior, a discussion of the characterization of these metastructures, and a discussion on how these different metastructures behave at different length scales (that is, periodicity and inclusion size relative to the wavelength of interest).

1.2 Electromagnetic behavior of ordinary materials

Before we discuss the behavior of engineered materials and how this behavior changes at different wavelength scales, we need to first discuss electromagnetic material properties, in general. We start by revisiting how the permittivity and permeability of a medium arise. Permittivity is due to the induced electric-dipole response of a large number of small particles [35, pp. 159–162]. Classically, these particles have been regarded as atoms or molecules, but in the past 70 years so-called artificial dielectrics have been developed whose "atoms" are small metal or dielectric objects, of dimensions large compared to atomic size, but still small compared to the wavelength of the electromagnetic waves acting in the "host" medium in which these inclusions are embedded [2,3,36–46]. In either case, the induced dipole moments are related by the electric polarizabilities of the scatterers to the electric field acting on each one. The dipole moments are then volume-averaged into a polarization density **P**, and the electric field is likewise averaged into a macroscopic or effective field **E**. From these, the electric displacement vector **D** and permittivity ϵ are defined by:

$$\mathbf{D} = \epsilon_0 \mathbf{E} + \mathbf{P} = \epsilon \mathbf{E}\,,$$

where ϵ is related to the electric polarizability densities of the scatterers in space.

Permeability originates in an analogous way from the volume density **M** of magnetic dipole moments arising from the angular momentum of charge due to particle spin and orbital movement, and is related to the magnetic polarizabilities of the scatterers. The effective fields **H** and **B** are then related to each other by the expression:

$$\mathbf{B} = \mu_0 \left(\mathbf{H} + \mathbf{M}\right) = \mu \mathbf{H}\,,$$

where μ is related to the magnetic polarizability densities of the scatterers in space.[1] We will denote the relative permittivities and permeabilities by a subscript r, and express ϵ and μ in terms of their real and imaginary parts by: $\epsilon = \epsilon_0(\epsilon_r' - j\epsilon_r'')$ and $\mu = \mu_0(\mu_r' - j\mu_r'')$ [Note that throughout this chapter the time dependence is $e^{j\omega t}$]. In this description, details of the field behavior on the scale of scatterer size and separation are lost, and indeed are often not of practical interest.

The problem of effective-medium theory and modeling the electromagnetic response of inclusions embedded in a medium is known as the "classical composite medium" and has a long history [2,3,36–46]. In recent years, artificial materials formed from periodic arrays of unusually-shaped conducting scatterers have been designed so as to have negative μ_r' and ϵ_r' (i.e., $\mu_r' < 0$ and $\epsilon_r' < 0$) and were given the name metamaterials [5–32]. Sufficiently deep within such a material, and if the frequency is low enough for scatterer spacing to be small compared to a wavelength, the medium appears to the average field as a continuous effective medium with some bulk effective material property. On the other hand, near the interface of such a material

[1] Scatterers of complex geometry can result in an anisotropic medium, for which ϵ and μ are tensors, or even in a *bianisotropic* medium, for which **D** and **H** are each affected by both **E** and **B**. We limit our attention in this paper to isotropic, non-bianisotropic composite materials.

with another medium, the fields acting on the scatterers that make up the material are expected to be differnet from deep within the bulk material, and the magnitude of this effect is uncertain [47].

For passive materials, $\mu_r'' \geq 0$ and $\epsilon_r'' \geq 0$. The real parts of the material parameters (i.e., μ_r' and ϵ_r') for many common materials are positive, but there are exceptions. We will see that negative permittivity and permeability are possible in composite/engineered materials. However, negative permittivity and permeability can occur at a more fundamental level. For example, in plasmas the combination of ordinary displacement current density with electron-convection current density can yield a net negative real part of the permittivity for sufficiently low frequencies [35, pp. 309–319]. Indeed, Rotman [42] has shown how an artificial dielectric can reproduce such a negative permittivity and serve as a model for a plasma. A transmission-line equivalent circuit for describing a plasma is discussed in [48]. Negative permittivity also appears near a resonance frequency in Lorentz's theory of dispersion (see [4], for example).

When one (but not both) of ϵ_r' or μ_r' is negative, plane waves decay exponentially, like modes below cutoff in a waveguide. However, when both ϵ_r' and μ_r' are negative, waves can still propagate in such a medium since the product $\mu\epsilon$ remains positive. In this case, we have a "backward wave", for which the phase of the wave moves in the direction opposite from that of the energy flow. For lossless media, this means that the phase velocity and group velocity have opposite signs.

1.3 Metamaterials and periodic composites: length-scale effects

Let us now discuss the global behavior of a periodic composite material. Depending on the wavelength and the periodicity of the inclusions that make up a composite material, the composite may or may not behave as an effective medium. Metamaterials are commonly engineered by designing specifically shaped scatterers/inclusions or other objects, placed throughout a volume to achieve a desirable bulk behavior of the materials. In these types of engineered materials the scatterers can be of various length scales: the dimensions of the scatterers can range from relatively large to nanometer size and even smaller, depending on the frequencies of interest. In some of these situations, the scatterers and the spacing between them can become comparable to the wavelength of the electromagnetic waves [specifically, the wavelength in the "host" medium in which these inclusions (scatterers) are embedded, or the wavelength in the inclusions]. In natural materials, where the inclusions are atoms or molecules, this does not happen until frequencies reach the x-ray region. But with artificial materials, this can happen at much lower frequencies and one has to revisit the notion of electromagnetic material properties. In fact, the electromagnetic field interaction with these types of engineered materials falls into three separate regions of behavior (see Fig. 1.3), with distinctive behaviors in each region. It is important to be aware of this and to understand the behavior in each region when either performing measurements or analyzing metamaterials at different length scales and/or frequencies, as will be described in the following subsections.

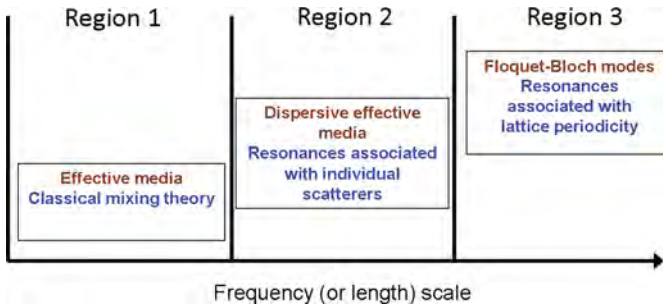

Figure 1.3 Three characteristic regions of composite materials or metamaterials.

1.3.1 Effective media: classical mixing theory

The first region in Fig. 1.3 corresponds to that of quasi-static behavior. This implies low frequencies—or specifically, frequencies where the wavelength is much larger than the lattice constant of the structure, that is, compared to the period of the scatterers that compose the composite medium, as well as the size of the inclusions. These scatterers could correspond to induced or permanent dipole moments, as is the case for atoms or molecules for classical materials, or could be generic in shape and placed in a host matrix to obtain an artificial composite material designed to have some desirable property. Using asymptotic techniques it is possible to show that the electromagnetic field in this low frequency limit sees the composite material as an equivalent effective medium with homogeneous material properties. The effective material properties are obtained from quasi-static field solutions of the periodic structure [49,50]. The basic result is that the effective permittivity is obtained by taking the ratio of some averaged D-field to an averaged E-field (as discussed above). The effective permeability is likewise obtained by taking the ratio of an averaged B-field to an averaged H-field.

The problem of effective-medium theory and modeling of electromagnetic response to an array of inclusions embedded in a host material has a long history going back to Maxwell, Rayleigh, as well as Poisson, Clausius and Mossotti before that. Much work has been done since then to compute the effective properties of homogeneous composite materials. A survey of this work can be found in [36,37,41]. The formulas for the effective properties given throughout the literature take on many forms. These range from simple bounds [41,51–53] to elaborate closed-form approximate formulas [36–38,41,43–45]. Note that these types of mixing formulas are only valid when the period of the structure is small in comparison to the wavelength of the electromagnetic wave. The reason for this is discussed in Section 1.3.2.

Let us look at a composite structure composed of particles embedded in a host matrix (shown in Fig. 1.4 for the case of spherical particles) in order to illustrate the implications of these classical mixing formulas (that is, the static limit). The Hashin–Shtrikman (HS) upper ($\epsilon_{\mathrm{HS}}^{U}$) and lower ($\epsilon_{\mathrm{HS}}^{L}$) bounds [51] are the best obtainable bounds using only the material parameters ϵ_1 (host matrix material), ϵ_2 (the material of the inclusion), and the fill factor g (volume fraction of space occupied by the bulk inclusion ϵ_2). They apply to composites based on inclusions of arbitrary shape. For a

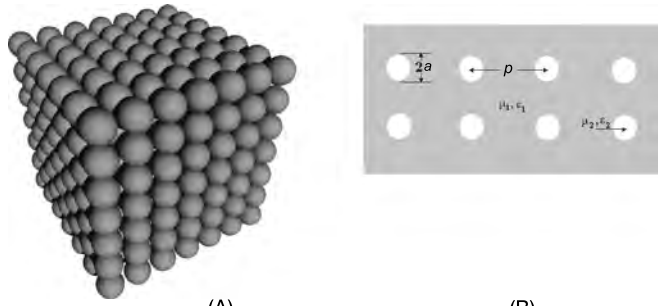

Figure 1.4 Composite structure containing spherical particles: (A) three-dimensional view and (B) cutaway view (from C.L. Holloway, E.F. Kuester, J. Baker-Jarvis, P. Kabos, A double negative (DNG) composite medium composed of magneto-dielectric spherical particles embedded in a matrix, IEEE Trans. Antennas Propag. 51 (10) (2003) 2596–2603, © 2003 IEEE).

three-dimensional composite material in which $\epsilon_2 > \epsilon_1$, the bounds are defined as

$$\epsilon_{\mathrm{HS}}^{L} \equiv \epsilon_1 + \frac{g}{\frac{1}{\epsilon_2-\epsilon_1} + \frac{1-g}{3\epsilon_1}}, \qquad \epsilon_{\mathrm{HS}}^{U} \equiv \epsilon_2 + \frac{1-g}{\frac{1}{\epsilon_1-\epsilon_2} + \frac{g}{3\epsilon_2}}. \tag{1.1}$$

If $\epsilon_2 < \epsilon_1$, the lower bound in Eq. (1.1) becomes an upper bound, and the upper bound becomes the lower bound (see [51] for details). Note that the expressions for these bounds need to be modified for other types of composite materials [41,50]. The variation of the effective permittivity (ϵ_{eff}) based on the expressions given in Eq. (1.1) is shown as a function of g ranging from 0 to 1 in Fig. 1.5 for two different values of the inclusion permittivity. Although results in this figure are shown for g approaching 1, for specific inclusion shapes, the limit $g = 1$ may not be achievable. For example, in the array of spheres, the spheres touch each other when $g = \pi/6$, and larger values of g have no meaning in this case.

For the composite shown in Fig. 1.4, Lewin [38] made a notable study of the effective permittivity and permeability μ_{e} and ϵ_{e}, by incorporating the solution of a boundary-value problem for scattering by a sphere into a unit cell, and then assuming that the medium is composed of a large number of these cells. For an array of lossless magneto-dielectric spheres, the relative effective μ'_{re} and ϵ'_{re} were found to be

$$\epsilon'_{\mathrm{re}} = \epsilon_{\mathrm{eff}} = \epsilon_{r1}\left(1 + \frac{3g}{\frac{F(\theta)+2b_e}{F(\theta)-b_e} - g}\right) \tag{1.2}$$

and

$$\mu'_{\mathrm{re}} = \mu_{\mathrm{eff}} = \mu_{r1}\left(1 + \frac{3g}{\frac{F(\theta)+2b_m}{F(\theta)-b_m} - g}\right). \tag{1.3}$$

In these expressions, μ_{r1} and ϵ_{r1} are the relative permeability and permittivity of the matrix (host) medium, μ_{r2} and ϵ_{r2} are the relative permeability and permittivity of the

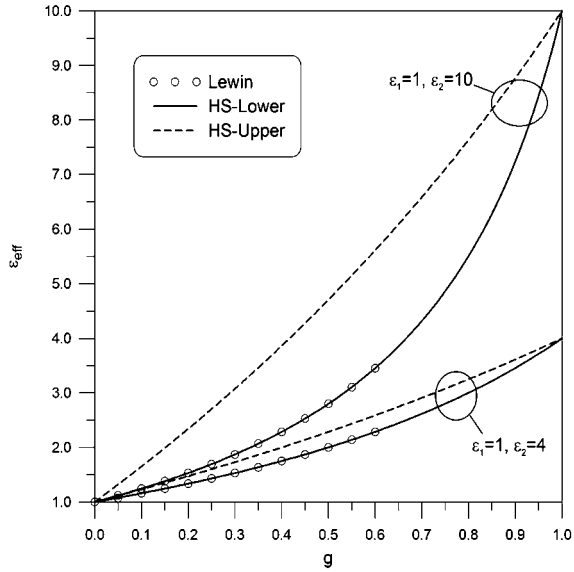

Figure 1.5 Effective properties of a spherical particle composite.

inclusions where

$$b_e = \frac{\epsilon_1}{\epsilon_2}, \qquad b_m = \frac{\mu_1}{\mu_2}. \tag{1.4}$$

The volume fraction g of the spherical inclusions is given by

$$g = \frac{4\pi a^3}{3p^3}, \tag{1.5}$$

where a is the particle radius and p is the particle spacing. The function $F(\theta)$ is

$$F(\theta) = \frac{2\,(\sin\theta - \theta\cos\theta)}{(\theta^2 - 1)\sin\theta + \theta\cos\theta}, \tag{1.6}$$

where

$$\theta = k_0 a \sqrt{\epsilon'_{r2}\mu'_{r2}} \tag{1.7}$$

and the free-space wavenumber is $k_0 = 2\pi/\lambda$, λ being the free-space wavelength. In the static limit $\theta \to 0$ (which implies no resonances in the inclusions), $F(\theta) \to 1$, and Lewin's formulas reduce to the Hashin–Shtrikman (HS) lower bounds, as can be observed in Fig. 1.5. Note that the results from Lewin's formula are only plotted to $g = \pi/6$, for the reason stated in the previous paragraph.

These results are typical of any mixing formula that one might choose to use for any type of composite material, in that a monotonic change takes place from the bulk

properties of the host towards the bulk properties of inclusion as the filling factor g increases from 0. Keep in mind that some mixing formulas may be more accurate than others depending on the geometry of the composite [36,37,41,49,50], but in general this trend is universal. This will be seen to be quite different from what occurs in the resonant effective material properties region (the second region in Fig. 1.3), which we will discuss in subsection 1.3.3. Notice also that there is no frequency dependence in the mixing formulas that we have discussed so far. The formulas are based on a quasi-static approximation, and the only frequency dependence that could occur would be because the bulk material properties of the matrix or inclusions are frequency-dependent. This is not the case in the second region, where resonant effects of the scatterers are important. This also will be discussed in subsection 1.3.3.

1.3.2 Floquet–Bloch modes: frequency selective surfaces and photonic band gap structures

Before we discuss Region 2 in Fig. 1.3, let us examine Region 3. In this region, the wavelength approaches the period of a periodic structure, and the fields no longer 'see' the composite as an effective medium. At these frequencies, a more complicated field behavior exists and more elaborate full-wave modeling techniques to analyze the EM field interaction with the composite periodic structures must be used. The classical approach that is used to analyze periodic structures is the Floquet–Bloch-mode approach [54–56]. To understand this method, we first review how fields in a homogeneous medium are expressed.

A plane wave is a solution of Maxwell's equations in a uniform, source-free region of space characterized by the material constants μ and ϵ. A typical component of (say) the electric field is given by

$$E = E_0 e^{-j(k_x x + k_y y + k_z z)}, \tag{1.8}$$

where E_0 is a constant amplitude, and the constants k_x, k_y and k_z are components of a wave-vector indicating the direction of propagation of the wave. All of the field components (**E** and **H**) have the same (x, y, z) dependence as in (1.8), but with different amplitudes. If the field is not identically zero, these amplitudes are related to each other by constraints imposed by Maxwell's equations; in addition, at a given frequency ω, the components of the wave-vector must obey

$$k^2 = \omega^2 \mu \epsilon = k_x^2 + k_y^2 + k_z^2 . \tag{1.9}$$

More general fields are representable by a superposition of plane-wave fields, either a sum or an integral over suitable sets of possible values of k_x, k_y, and $k_z = \sqrt{k^2 - k_x^2 - k_y^2}$. Those plane waves for which $k_x^2 + k_y^2 > k^2$ are evanescent in the z-direction and do not contribute significantly in the far field when z is large enough.

For a three-dimensional periodic medium, when μ and ϵ are periodic functions of x, y, and z, with periods p_x, p_y, and p_z, respectively, a Floquet–Bloch mode for a

component of the E-field has the form

$$E = E_p(x, y, z)e^{-j(k_x x + k_y y + k_z z)}, \tag{1.10}$$

where E_p is a function periodic in x, y and z with the same periods as μ and ϵ. As with the plane-wave solution, the constants k_x, k_y, and k_z and the amplitude functions E_p, etc., cannot take on arbitrary values, but are constrained by the requirement that the field is nontrivial and obeys Maxwell's equations. For given values of k_x, k_y, and k_z, this can happen only when the frequency ω is equal to one of a set of *eigenfrequencies* $\omega_r(k_x, k_y, k_z)$. The relation between components of the wave-vector is then the implicit equation $\omega = \omega_r(k_x, k_y, k_z)$, which generalizes (1.9). The periodic function E_p can be represented as a complex exponential Fourier series:

$$E_p(x, y, z) = \sum_{l,m,n=-\infty}^{\infty} C_{lmn} e^{-j\left(\frac{2\pi l x}{p_x} + \frac{2\pi m y}{p_y} + \frac{2\pi n z}{p_z}\right)} \tag{1.11}$$

or

$$E = \sum_{l,m,n=-\infty}^{\infty} C_{lmn} e^{-j(k_{xl} x + k_{ym} y + k_{zn} z)}, \tag{1.12}$$

where

$$k_{xl} = k_x + \frac{2l\pi}{p_x}, \qquad k_{ym} = k_y + \frac{2m\pi}{p_y}, \qquad k_{zn} = k_z + \frac{2n\pi}{p_z}, \tag{1.13}$$

and $p_{x,y,z}$ are the lattice periods in the x, y, and z directions, respectively. The constants $C_{l,n,m}$ and eigenfrequencies $\omega_r(k_x, k_y, k_z)$ are determined by constraining the field to obey Maxwell's equations—this is usually done numerically.

Analogous to the plane-wave case, if $k_{xl}^2 + k_{ym}^2$ is large enough, the field will decay in the z-direction, and such waves will not contribute in the far field. It turns out that, for kp_x, kp_y, and kp_z smaller than about π (where k is now a suitably-defined representative wavenumber), only the lowest-order Floquet–Bloch mode (the one with the smallest value of $\omega_r = \omega_0$) can propagate without attenuation. Put another way, if the wavelength is large in comparison to the periods, only the lowest-order Floquet–Bloch mode propagates. As the frequency increases, more of the higher-order modes begin to propagate. For small periods and long wavelengths, the lowest-order Floquet–Bloch mode represents (in some sense) the averaged fields propagating through the composite periodic structure. These fields along with the eigenfrequency ω_0 allow us to determine an effective medium in terms of ϵ_e and μ_e.

The situation is quite different once the higher-order modes begin to propagate. No longer do unique values of ϵ_e and μ_e fully determine the non-evanescent field, and complicated interference effects among the Floquet–Bloch modes will arise. Certainly, important practical applications of these effects exist (Bragg scattering perhaps foremost among them), but a simplified effective-medium description is no longer possible. A field propagating through a composite sees the structure as an effective

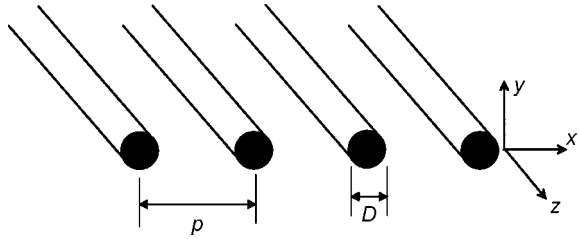

Figure 1.6 Infinitely-long metal wire grating in free space, where p is the period of the grating and D is the wire diameter.

medium as long as the higher-order Floquet–Bloch modes do not propagate into it. For a background medium of free space, the restriction on $k_0 p$ as a function of the plane-wave incidence angle ϕ for this to happen is

$$k_o p < \frac{2\pi}{1 - \sin\phi}.$$

Periodic structures used in such higher-frequency applications have been given various names throughout the literature. In recent years, high-frequency periodic surfaces have been given the name frequency-selective surfaces (FSSs) [57,58] (historically known as periodic gratings) and high-frequency three-dimensional periodic materials have been given the name photonic band gap (PBG) materials [5,59]. FSS and PBG structures have similar characteristics, that is, at certain frequencies the FSS and PBG can block the propagation of an EM wave. The frequency bands where this blocking effect occurs are referred to as stopbands. At other frequencies, the periodic structure allows energy to propagate through the structure; these frequency bands are referred to as passbands.

This can be readily seen by considering the infinitely-long metal wire grating shown in Fig. 1.6. The transverse electric (TE) reflection and transmission coefficients of this two-dimensional wire grating in free space are shown in Fig. 1.7. These results were obtained with a finite-element numerical program. These quantities are a complicated function of the lattice configuration (e.g., the period p and diameter D of the wires). The lattice will severely attenuate the transmitted field at wavelengths that are much larger than the lattice period p. In general, the attenuation of the fields due to the lattice is monotonic and decreases with frequency up to the first resonance (i.e., the peak in the transmitted field). For example, Fig. 1.7A shows results for a lattice in free space, where $p = 7.62$ cm and $D = 1.91$ cm, and Fig. 1.7B shows results for a lattice in free space, where $p = 15.24$ cm and $D = 5.08$ cm.

At low frequencies, the lattice acts inductively and the transmitted field strength increases with frequency to a maximum at the first resonance with the wavelength (i.e., $\lambda \approx p$). It should be noted that the shape of the curves as well as the wavelength at the first resonance are, in general, a function of the wire diameter as well as the period. The first resonance occurs when $\lambda \approx p$ (and not $\lambda/2 \approx p$), because the plane-wave excitation causes currents to flow in the same direction on adjacent parallel conducting elements of the lattice that are aligned with the incident electric field. Since the

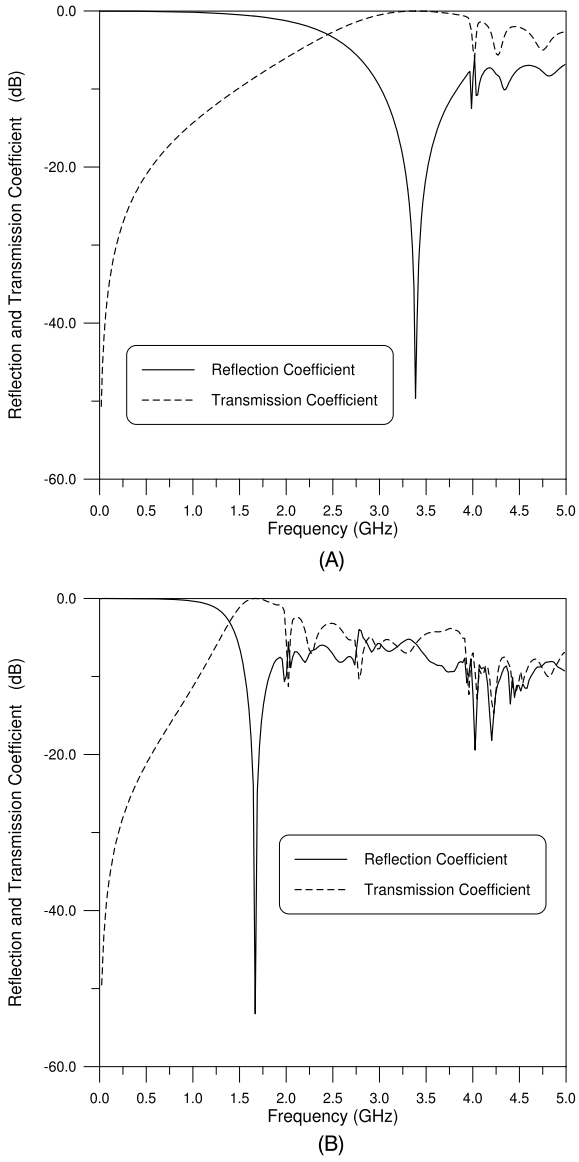

Figure 1.7 TE reflection and transmission characteristics of a two-dimensional array of infinitely-long metal wires: (A) $p = 7.62$ cm and $D = 1.91$ cm, (B) $p = 15.24$ cm and $D = 5.08$ cm. These results are for normal incidence.

currents on two adjacent conductors are equal in magnitude and direction, there is a null in the induced magnetic and electric fields halfway between the conductors which is consistent with this mode. From these results, we see that there is a passband when $\lambda \approx p$. Similar types of results are seen for different types of periodic structures, that

is, stopbands and passbands will develop in the structure (FSS and PBG structures; see [5,57–59]).

These effects of constructive and destructive interference of the various modes as the wave propagates through the composite, are what give rise to the unique characteristics of FSS and PBS structures. It is important to note that such effects cannot be represented or captured by an effective-media theory. These stopband and passband effects of FSS and PBG structures are caused by resonances associated with the periodicity of the structure. In Section 1.3.3 we see that resonances associated with the scatterers themselves can cause interesting and unexpected effects in the effective material properties of a composite.

1.3.3 Effective media: scatterer resonances

Resonant features of the scatterers (or inclusions) that compose an effective medium provide us the power to engineer the medium's permittivity and/or permeability in order to achieve unique and interesting properties. Region 2 in Fig. 1.3 corresponds to a region where the scatterers are designed in such a manner (either via their shape or bulk material properties) such that the scatterers themselves can resonate. When this occurs, so-called metamaterials can be realized.

When the scatterers are non-resonant, the real parts of the material parameters (i.e., μ_r' and ϵ_r') for the engineered materials are usually positive, but there are exceptions, as discussed in Section 1.2. When the scatterers are resonant, negative permittivity and permeability are possible in composite materials. Materials of this type are also called "double" negative (DNG) media, negative-index materials, backward-wave media (BW), or left-handed materials. This kind of material is just one of many types of metamaterials. Early investigators in the fledgling area of metamaterials attributed the first study of such media to Veselago [12] in 1967, but Lamb [60] in 1904, Schuster [61] in 1904, Pocklington [62] in 1905, Mandel'shtam [63,64] in 1945, Malyuzhinets in 1951 [65] and Sivukhin in 1957 [66] had all previously discussed the properties of wave propagation in backward-wave media. Some other historical (or "pre-historical") surveys have been given in [15,67–69]. More recently, many other authors [5–32] have studied the properties and potential applications of DNG materials in detail. Also see [70–76].

Much of the early work on DNG materials concentrated on metallic inclusions [5–32]. An interesting question is: "Can the DNG material effect occur in a pure dielectric or magneto-dielectric composite medium?" To address this question, we refer back to the work of Lewin [38], in which he used Mie's exact solution of the problem of scattering by a material sphere to derive an expression for the effective properties of an array of spherical particles embedded in a background matrix (although many of his results had already been obtained, albeit in a much more cumbersome form, by previous researchers [39,40]). Lewin's work showed that when the size of the spherical scatterers is not small compared to a wavelength *in the material of the scatterers* (but *is* small compared to a wavelength in the matrix material), μ_e and ϵ_e become frequency-dependent. The expressions for the effective permittivity and permeability are presented in Eqs. (1.2) and (1.3). The interesting parameter in these equations is

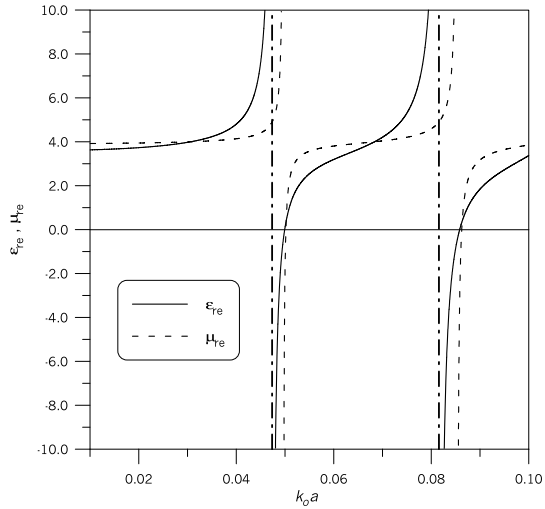

Figure 1.8 ϵ_{re} and μ_{re} for an array of spheres with $g = 0.5$, $\epsilon'_{r1} = \mu'_{r1} = 1$, $\epsilon'_{r2} = 40$, and $\mu'_{r2} = 200$. The dashed-dot lines represent the asymptotes for ϵ_{re}. From C.L. Holloway, E.F. Kuester, J. Baker-Jarvis, P. Kabos, A double negative (DNG) composite medium composed of magneto-dielectric spherical particles embedded in a matrix, IEEE Trans. Antennas Propag. 51 (10) (2003) 2596–2603, © 2003 IEEE.

the factor $F(\theta)$. In section 1.3.1, the quasi-static of $F(\theta)$ is emphasized. In that static limit $F(\theta) \to 1$. From Eq. (1.6) and plots shown in [29], it is apparent that $F(\theta)$ has a resonant behavior. The possibility of such a composite structure (a pure dielectric or magneto-dielectric composite) having both negative effective permittivity and permeability was first demonstrated in [29], where the conditions that must be met for the effective permittivity and permeability to be negative were given.

In [29] it is shown that these conditions can be met with realistic bulk material properties of the matrix and the spherical inclusions. For example, Fig. 1.8 shows results for $g = 0.5$, $\epsilon'_{r1} = \mu'_{r1} = 1$, $\epsilon'_{r2} = 40$, and $\mu'_{r2} = 200$ as a function of $k_0 a$ (where a is the radius of the spheres and k_0 is the free-space wavenumber). Between $0 \leq k_0 a \leq 0.1$ there are two regions where both μ'_{re} and ϵ'_{re} become negative, producing a negative-index material [29]. This negative-index behavior also occurs when $\epsilon'_{r1}/\epsilon'_{r2} = \mu'_{r1}/\mu'_{r2}$. Fig. 1.9 shows such a composite that has a bandwidth (bands where permittivity and permeability are simultaneously negative) of 10 %. Fig. 1.10 shows results for the real and imaginary part of ϵ_{re} for an array of lossy spherical particles. The results in this figure are for different values of the dielectric loss tangent of the spherical particles, defined as $\tan\delta = \epsilon''_r/\epsilon'_r$. Notice that, for this example, the real part of the effective permittivity can still be negative for loss tangents as large as 0.04. However, for larger values of $\tan\delta$ the resonance is damped out and the real part of the effective permittivity remains positive. This shows that if the inclusion (i.e., the spherical particle) becomes too lossy, DNG properties cannot be realized. While large values of negative properties can be attained near resonance as shown in Fig. 1.10A, working too near these resonances has an adverse feature. The imaginary part of ϵ_{eff} shown in Fig. 1.10B illustrates an important aspect of using metamaterials too close to

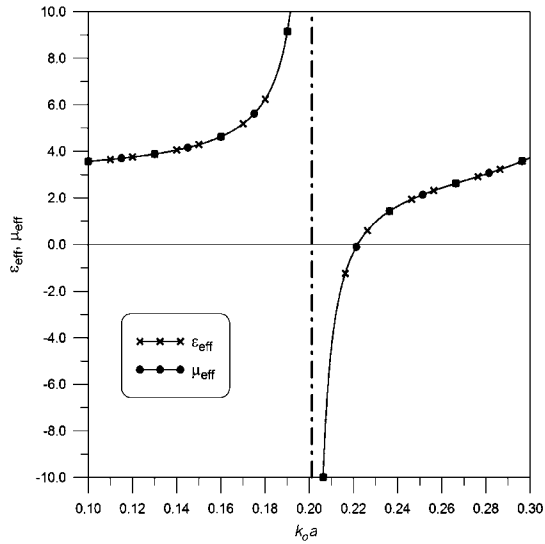

Figure 1.9 ϵ_{re} and μ_{re} for an array of spheres with $g = 0.5$, $\epsilon'_{r1} = \mu'_{r1} = 1$, $\epsilon'_{r2} = 20$, and $\mu'_{r2} = 20$. The dashed-dot line represents the asymptote. Notice that ϵ_{re} and μ_{re} are identical. From C.L. Holloway, E.F. Kuester, J. Baker-Jarvis, P. Kabos, A double negative (DNG) composite medium composed of magneto-dielectric spherical particles embedded in a matrix, IEEE Trans. Antennas Propag. 51 (10) (2003) 2596–2603, © 2003 IEEE.

a resonance, in that losses can be very large near the resonance. As a result, researchers have been investigating and designing metamaterials away from these resonances. Tailoring materials to a desired value and near-zero index materials are two examples of metamaterial applications for frequencies away from resonance.

Once it was demonstrated in [29] that metamaterials composed of dielectric spherical inclusions were possible, other dielectric and magneto-dielectric inclusions started appearing as a means to develop DNG materials and other desirable properties. This includes layered-spherical particles, arrays of different sized spheres, cylindrical and cubic inclusions, as well as other geometries [30,77–94].

The negative material properties are a result of the resonances associated with the scatterers that make up the composite material. Therefore, it should not be a surprise that any scatterer that can resonate can be used to obtain the DNG effect. In fact, the Lewin approach can be readily extended to other geometries and to other types of inclusions. Khizhniak wrote a series of papers [43–45] in which he generalized Lewin's model and presented expressions for the effective material property tensors of an artificial material formed by an array of scatterers with arbitrary geometric shapes. Khizhniak presents expressions for the effective material properties that have the same functional behavior as Lewin's and does indeed suggest that negative material properties can be obtained via arbitrarily shaped inclusions. Recently, several papers have studied the problem of designing engineered artificial materials with negative μ'_r and ϵ'_r formed from periodic arrays of unusually-shaped conducting scatterers, in particular, split metal rings and posts [5–28,31,32,95]. These structures

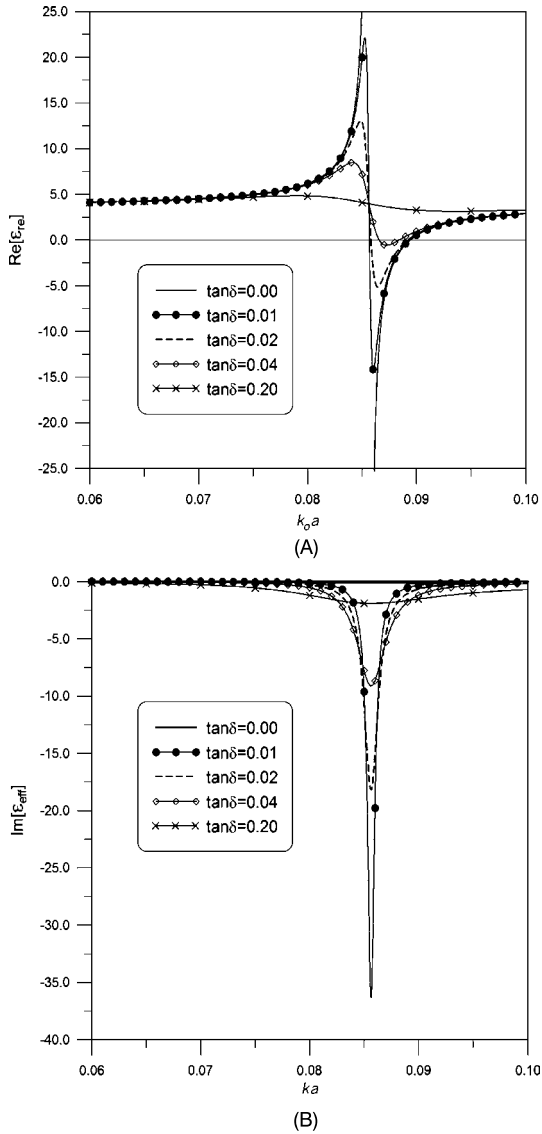

Figure 1.10 Array of lossy spherical particles: ϵ_{re} and μ_{re} for $g = 0.5$, $\epsilon'_{r1} = \mu'_{r1} = 1$, $\epsilon'_{r2} = 50$, and $\mu'_{r2} = 50$: (A) real part for ϵ_{re} (from C.L. Holloway, E.F. Kuester, J. Baker-Jarvis, P. Kabos, A double negative (DNG) composite medium composed of magneto-dielectric spherical particles embedded in a matrix, IEEE Trans. Antennas Propag. 51 (10) (2003) 2596–2603, © 2003 IEEE) and (B) imaginary part for ϵ_{re}.

can be quite complicated to fabricate when compared to composites composed of the magneto-dielectric inclusions.

Since these conducting scatterers are essentially resonant structures, the goal is to design the microfabricated resonant circuits with desired effective properties in a unit

cell. The design of such a structure was described in detail in [18]. The design is based on the averaging of the magnetic field components along the axes of the unit cell. Pendry averages the magnetic field in a cube of side $a(= p_x = p_y = p_z)$. For each magnetic field component

$$< H >_i = \frac{1}{a} \int_{r_i} \mathbf{H} \cdot d\mathbf{r}, \tag{1.14}$$

the induction field is averaged as

$$< B >_i = \frac{1}{a^2} \int_{S_i} \mathbf{B} \cdot d\mathbf{S}, \tag{1.15}$$

where $i = x$, y, or z, r_i is a path from the origin to $p_i \mathbf{a}_i$, $\mathbf{a}_i$ is a unit vector in the direction i, and S_i is a square of side a in the plane $i = 0$. Following these averaging definitions the effective permeability is then defined as

$$\mu_{\text{eff}(i)} = \frac{< B >_i}{\mu_0 < H >_i}. \tag{1.16}$$

The effective permittivity is given by a similar expression

$$\epsilon_{\text{eff}(i)} = \frac{< D >_i}{\epsilon_0 < E >_i}. \tag{1.17}$$

For negative permittivity or permeability, the equivalent circuit of the scatterer circuit has to be resonant, which requires the introduction of capacitance into the inductive system (or vice versa). Pendry introduced the capacitance through gaps in coupled-ring resonators; details are discussed in [18]. Any microstructured microwave resonant device, passive and/or active, can in principle be used to produce a desired effective permeability in a periodic structure designed for double-negative applications [31].

The most convenient (and traditional) method to model metamaterials is with effective-medium theory. It should be emphasized that the averaging (or homogenization, or effective material model presentation) is valid only when the wavelength is large compared to the lattice constant of the period cell. While period cell averaging for the fields is the correct method for defining effective material properties, most researchers in practice use an approach where they obtain the reflection and transmission properties (either through measurements or numerical simulations) of a metamaterial consisting of several layers (sometimes as few as three). The term "layer" means a plane of scatterers with an associated thickness. When referring to the layers of a metamaterial, the thickness is the period of the bulk materials in the direction perpendicular to the plane of scatterers. Once the reflection and transmission properties are obtained, a Nicolson–Ross–Weir (NRW) approach [96,97] is used to obtain the effective material properties of the bulk metamaterials. Note that the standard NRW approach must be modified when negative material properties exist; typically, the choice of the sign of a square-root is made unambiguous by ensuring

positive power flow [98–102]. In general, for a bulk three-dimensional material (with five layers or more) the approach results in unique effective material properties for the metamaterials. However, there are conditions where these modified NRW approaches fail; for details see [47,100,101], and [103]. This failure manifests itself in a dependence of the extracted bulk electromagnetic material parameters on the thickness of the sample used [98,104–106].

If used properly, the effective material approach can be a self-consistent and unique method for characterizing a metamaterial. That is, no matter what thickness of the same metamaterial is modeled (i.e., no matter the number of layers that compose the metamaterial), the same values for the bulk effective material properties should be obtained. By definition, a bulk property should not depend on the size (or shape, for that matter) of the material sample. True bulk properties of a material should be retrievable independent of the thickness of the sample chosen. Let us note here that some models of metasurfaces in terms of "bulk" properties are actually nonlocal–the obtained permittivity and permeability are spatially dispersive, dependent on the wavenumber of the wave propagating through the medium. This approach can address the issues raised here to some extent, but is more complicated to use, in general, than a local model. See, for example, [107].

Applications of DNG materials include, 1) shielding materials, 2) low-reflection materials, 3) substrate materials, 4) antenna applications, 5) electronic switches, 6) resonators, 7) controllable surfaces, 8) cloaking, and 9) the so-called perfect lens. When resonance is used to obtain some desired metamaterial behavior, a structure made from passive materials must exhibit dispersion and therefore loss. This is required by the Kramers–Kronig dispersion relations for the behavior to obey causality. As discussed above, losses are high near resonances, and as such, one typically avoids this region.

We need to emphasize that Region 2 in Fig. 1.3 does not always occur. The scatterers need to be designed so that the scatterers' resonances occur before the next higher-order Floquet–Bloch mode can propagate. For example, in the case of spherical particle inclusions, if the bulk properties and the radius of a spherical particle composite are too small, the scatterer resonances would be pushed toward the Floquet–Bloch-mode region and a DNG material would not be realized. The scatterer resonance region and the Floquet–Bloch-mode region would overlap and an effective-medium model would not capture the behavior of the composite material. Furthermore, if the size and shape of the inclusions (the dielectric structures used in [29,30,77–82] or metallic inclusions in [5–28,31], and [32]) are not chosen properly, then the resonance would be pushed into the Floquet–Bloch-mode region and once again DNG materials would not be realized. Similar effects are also discussed in [122].

In summary, in the first two regions, the electromagnetic field behaves as if the composite material is some type of effective medium. In region 1 (the classical mixing theory region) the effective material properties have no frequency dependence (except for that due to the constituent materials). In region 2 (the scatterer resonant region) the material behaves as an effective medium and has the inherent frequency dependence preserved in the effective material property model. In this region it is possible to achieve DNG materials and other desirable exotic material properties. Finally, for the last region (region 3 in Fig. 1.3), the electromagnetic field interaction with

the periodic structure is more complex. Scattering is the mechanism for the field behavior, and we can no longer think of the composite material simply as an effective medium. When the wavelength approaches the lattice constant, higher-order Floquet–Bloch modes must be considered. FSS and PBG are the predominant applications found in this region.

1.4 Metasurfaces

Metamaterials are engineered by arranging a set of scatterers throughout a three-dimensional region of space in a specific pattern so as to achieve some desirable bulk behavior of the material. This concept can be extended by judiciously placing scatterers in a two-dimensional pattern at a surface or interface. Such a surface version of a metamaterial has been given the name metasurface, and includes metafilms and metascreens (both of these subcategories will be discussed below) as special cases [33, 34,108–110]. Metasurfaces have also been referred to in the literature as single-layer metamaterials.

The simplicity and relative ease of fabrication of metasurfaces make them attractive alternatives to three-dimensional (3D) metamaterials. In many applications, metasurfaces can be used in place of metamaterials. Metasurfaces have the advantage of taking up less physical space than do full 3D metamaterial structures; as a consequence they can also offer the possibility of lower losses. The application of metasurfaces at frequencies from microwave to optical has attracted great interest in recent years [33,34, 115–159]. In addition to the applications mentioned above for metamaterials, metasurfaces allow for controllable "smart" surfaces, miniaturized cavity resonators, novel waveguiding structures, compact and wide-angle absorbers, impedance matching surfaces, biomedical devices, tailoring wave fronts, polarization conversion, antennas, and high speed switching devices, to name only a few.

We will call any periodic two-dimensional structure whose thickness and periodicity are small compared to a wavelength in the surrounding media a metasurface. Within this general designation, we can identify two important subclasses. Metasurfaces that have a "cermet" topology, which refers to an array of isolated (non-touching) scatterers (Fig. 1.11), are called metafilms [33] and [108] (a term coined in [110] for such surfaces). Metasurfaces with a "fishnet" structure (Fig. 1.12) are called metascreens [33,109]. These metascreens are characterized by periodically-spaced apertures in an otherwise relatively impenetrable surface. Other kinds of metasurfaces exist that lie somewhere between these two extremes. For example, a grating of parallel conducting wires (a metagrating) behaves like a metafilm to electric fields perpendicular to the wire axes, but like a metascreen for electric fields parallel to the wire axes [112]. It is important to note that the individual scatterers constituting a metafilm (or apertures constituting a metascreen) are not necessarily of zero thickness (or even small compared to the lattice constants); they may be of arbitrary shape, and their dimensions are required to be small only in comparison to a wavelength in the surrounding medium, which is true *a fortiori* because the lattice constant has been assumed small compared to a wavelength.

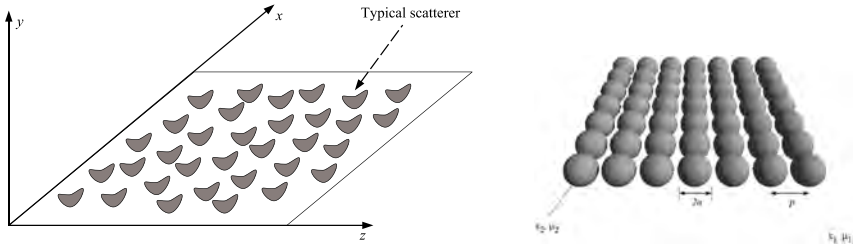

Figure 1.11 Metafilm examples: (A) array of arbitrary shaped scatterers and (B) array of spherical particles. Parts (A) and (B) from C.L. Holloway, E.F. Kuester, J.A. Gordon, J. O'Hara, J. Booth, D.R. Smith, An overview of the theory and applications of metasurfaces: the two-dimensional equivalents of metamaterials, IEEE Antennas Propag. Mag. 54 (2) (April 2012) 10–35, © 2012 IEEE.

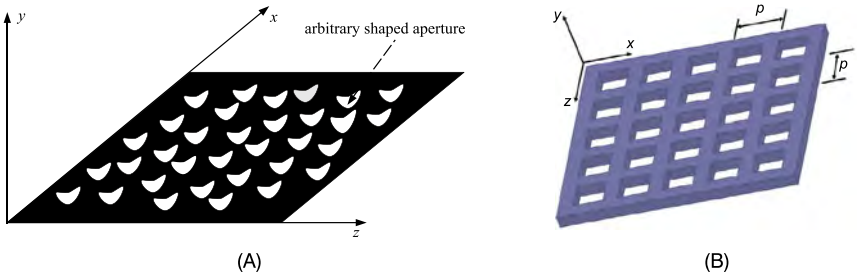

Figure 1.12 Metascreen examples: (A) array of arbitrary shaped apertures and (B) array of square apertures. Parts (A) and (B) from C.L. Holloway, E.F. Kuester, Generalized sheet transition conditions (GSTCs) for a metascreen, IEEE Trans. Antennas Propag. 66 (5) (2018) 2414–2427, © 2018 IEEE.

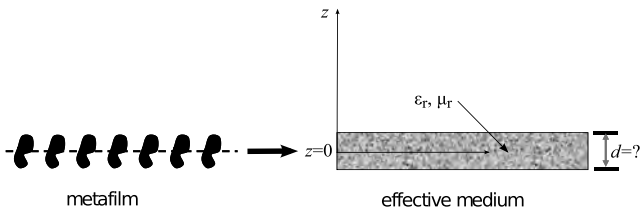

Figure 1.13 Representing a metafilm as an effective medium with thickness d. From C.L. Holloway, E.F. Kuester, A. Dienstfrey, Characterizing metasurfaces/metafilms: the connection between surface susceptibilities and effective material properties, IEEE Antennas Wirel. Propag. Lett. 10 (2011) 1507–1511, © 2011 IEEE.

Similar to metamaterials, depending on the wavelength-to-period spacing, three regions of behavior will occur for EM interactions with a metasurface. For a two-dimensional lattice of scatterers or apertures, region 1 in Fig. 1.3 corresponds to classical thin-film materials, while region 3 in Fig. 1.3 corresponds to resonances associated with the periodicity of the scatterers/apertures. The conventional FSS and PBG [57–59] fall into this third region. On the other hand, when we talk about a metasurface, we are referring to an array of scatterers/apertures that lies in region 2 (or even region 1). Resonances of the surface may be associated with the resonances of

the scatterers/apertures, but not with the periodicity of the array. Ordinary frequency-selective surfaces are sometimes operated in this regime, but the distinction between this type of operation and that of region 3 has not usually been made.

We emphasize that, as for the case of a metamaterial, region 2 in Fig. 1.3 may not always occur for a metasurface. The scatterers/apertures need to be properly designed, such that the scatterers' resonances occur at a frequency well below that where the next higher-order Floquet–Bloch mode can propagate. For example, if the bulk properties and the radius of a spherical-particle composite (see [29]) are too small, or if the sizes or shapes of the scatterers used in the material are not properly chosen, the scatterers' resonances would be pushed toward the Floquet–Bloch-mode region, and in this case an effective-medium model would not adequately describe the behavior of the composite material.

In summary, in regions 1 and 2 of Fig. 1.3 the interaction of an electromagnetic field with a metasurface is described by effective surface parameters of some kind, to be discussed below. In region 1 (analogous to the classical mixing theory region for the case of a metamaterial), the effective surface parameters are not frequency-dependent (except insofar as the constituent bulk properties have a frequency dependence). In region 2 (the scatterers' resonant region), the metasurface still is modeled by effective surface properties, which now may possess an inherent frequency dependence. In this region, it is possible to achieve interesting resonant behaviors. In the last region (region 3 in Fig. 1.3), the electromagnetic field's interaction with the periodic array is very involved. We may no longer think of the surface as behaving like an interface with effective surface parameters. When the wavelength approaches the period, higher-order Floquet–Bloch modes must be considered, and one typically does not refer to these structures as metasurfaces in this region.

1.4.1 Characterizing a metasurface

Like a metamaterial, the behavior of a metafilm is determined by the electric and magnetic polarizabilities of its constituent scatterers (or its constituent apertures for a metascreen). The traditional and most convenient method by which to model metamaterials is with effective-medium theory. Attempts to use a similar bulk-parameter analysis for metasurfaces have been less successful (see [113], [33], and [114] for a detailed discussion on this point). Indeed, some previous metafilm studies have modeled the film as a single-layer metamaterial in which effective bulk material properties of the metasurface are obtained by forcing the introduction of an arbitrary non-zero thickness parameter into the analysis. As we will demonstrate, several problems arise from the physically artificial character of this parameter; the bulk property characterization of a metasurface is incorrect at a fundamental level. To the extent that classical algorithms for bulk-parameter extraction give results that depend on sample size, we would be forced to conclude that some localized effect is occurring near the boundary of the sample [47,100,101,110], analogous to the effect of cutoff modes near the junction between two different waveguides.

An equivalent-bulk layer representation of a metasurface is shown in Fig. 1.13. The problem is that the thickness of a metasurface would not be uniquely defined,

nor would the effective material properties. In [108,109,113,114], it is shown that the effective surface parameters of a metafilm/metascreen are unique properties of a metasurface and thus are the most appropriate way to characterize a metasurface. We will see below that the surface parameters correspond to what we will call effective surface susceptibilities (defined below as χ_{MS} and χ_{ES} for the magnetic and electric surface susceptibilities, respectively) for metafilms [33,108], and in addition so-called surface porosities (defined below as π_{MS} and π_{ES} for the magnetic and electric surface porosities, respectively) for metascreens [33,109]. Techniques for retrieving the surface susceptibilities for a given metasurface based on reflection and transmission measurements (or simulations) are presented in [33,113,114,117].

To illustrate the issue of representing a metasurface as a material with a bulk effective permittivity and permeability, we present in Fig. 1.14A retrieved values of ϵ_r (the effective permittivity) for an array of lossy spherical particles (radius $a = 10$ mm, period $p = 25.59$ mm, $\epsilon_p = 2$, $\mu_p = 900$, and $\tan\delta = 0.04$) for different values of the assumed thickness d. These results were obtained by computing numerical values of the reflection and transmission coefficients for this array of spheres and then using the modified Nicolson–Ross–Weir (NRW) method [98,99,102] for determining ϵ_r of the slab (see [114] for details). As expected, these results show a functional dependence of ϵ_r on d. Fig. 1.14B shows results for $d(\epsilon_r - 1)$ for different values of d. We have also plotted the retrieved values of the surface susceptibility χ_{ES}^{yy} (the first superscript "y" corresponds to the component of the surface susceptibility and the second superscript "y" corresponds to the polarization of the incident field; see [108] for details) for this array that appears in (1.18) below (also obtained from using retrieval algorithms and the numerical values of reflection and transmission coefficients [114]). The retrieved values for χ_{ES}^{yy} are the same as the analytical values given in [113]. The results shown in Fig. 1.14B illustrate that, for sufficiently low frequencies, $d(\epsilon_r - 1)$ is independent of d and identical to χ_{ES}^{yy}. Although the connection between surface susceptibilities and the effective bulk properties of a slab was not discussed explicitly in [27], Smith et al. [27] do allude to the fact that the product of the slab thickness and the effective material properties of the slab should be constant.

Additional examples of the surface susceptibilities for two different metafilm structures are shown in Fig. 1.15. One is an array of lossy spherical particles and the other is an array of thin metallic scatterers (Fig. 1.15D). As we will see below, a metascreen requires both surface susceptibilities and surface porosities to fully characterize the metascreen. Fig. 1.16 shows both surface susceptibilities and surface porosities for a metascreen composed of an array of square apertures.

When all is said and done, we would argue that a model for a metafilm that uses uniquely specified quantities (i.e., χ_{MS} or χ_{ES} as defined below) is more natural than an approach that involves two arbitrary quantities (d and ϵ_r). Likewise, for a metascreen we should use both surface susceptibilities and surface porosities as defined below [33,109]. Even though it has been shown that the electrical and magnetic surface susceptibilities are the most appropriate manner to characterize metafilms, some researchers continue to characterize them in terms of bulk effective material properties. If one insists on characterizing a metasurface as a thin material slab with bulk effective material properties and a thickness d, the only meaningful (and unique)

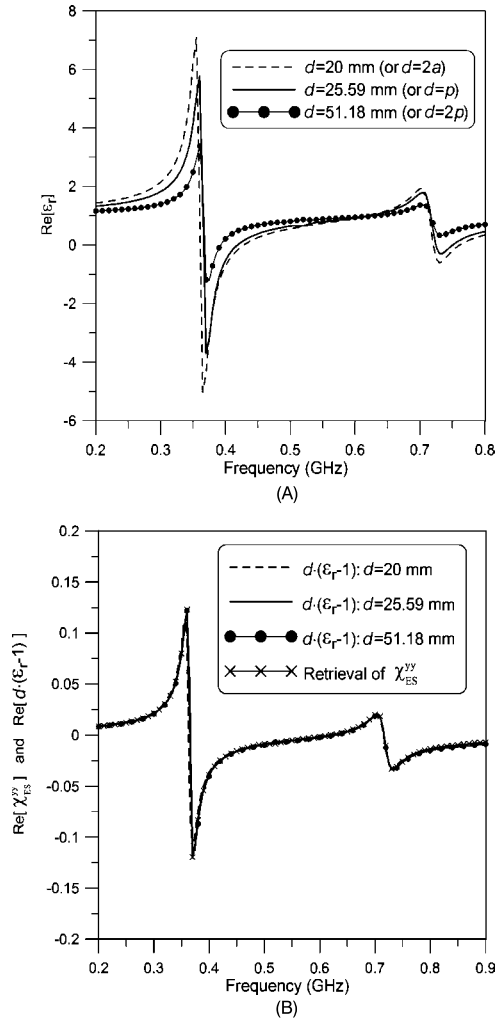

Figure 1.14 Results for an array of lossy spheres: (A) retrieved ϵ_r and (B) $d(\epsilon_r - 1)$ and χ_{ES}^{yy}. From C.L. Holloway, E.F. Kuester, A. Dienstfrey, Characterizing metasurfaces/metafilms: the connection between surface susceptibilities and effective material properties, IEEE Antennas Wirel. Propag. Lett. 10 (2011) 1507–1511, © 2011 IEEE.

parameters will be products such as $d(\epsilon_r - 1)$ and $d(\mu_r - 1)$, if the slab is centered at the plane containing the metafilm. A retrieval approach that gives unique quantities like χ_{MS} and χ_{ES} is more natural than one that merely gives products of otherwise undetermined quantities [33,113,114,117].

In contrast to the effective-medium description used for a metamaterial, boundary conditions incorporating the effective surface parameters (surface susceptibilities and surface porosities) of the metasurface are the best way to characterize it. These boundary conditions are called generalized sheet-transition conditions (GSTCs) [33,

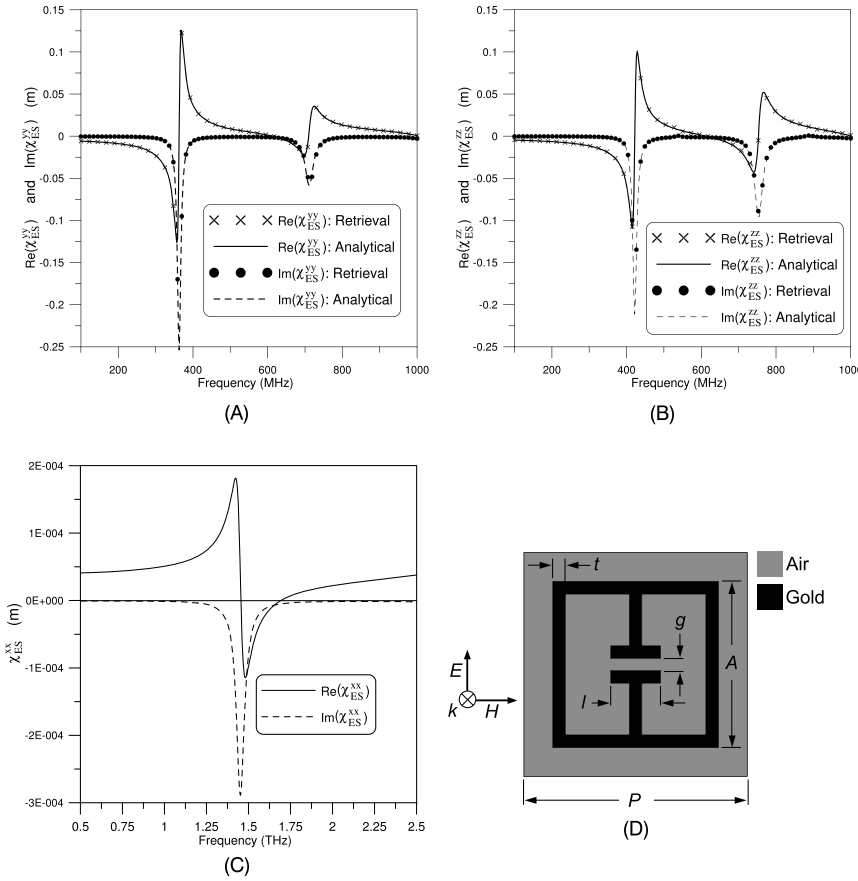

Figure 1.15 Surface susceptibilities for a metafilm composed of (A) χ_{ES}^{yy} for spherical particles ($a = 10$ mm, $p = 25.59$ mm, $\epsilon_r = 2$, $\mu_r = 900$, and $\tan\delta = 0.04$), (B) χ_{ES}^{zz} for the same array as in (A), (C) χ_{ES}^{zz} for an array of thin metallic scatterers shown in (D), and (D) thin metallic scatterer for electrical surface susceptibility ($t = 3$ μm, $A = 40$ μm, $p = 54$ μm, and $l = 12$ μm). Parts (A), (B), (C), (D) from C.L. Holloway, A. Dienstfrey, E.F. Kuester, J.F. O'Hara, A.K. Azad, A.J. Taylor, A discussion on the interpretation and characterization of metafilms-metasurfaces: the two-dimensional equivalent of metamaterials, Metamaterials 3 (2009) 100–112.

108–110]. The coefficients appearing in the GSTCs for any given metasurface are all that are required to model its macroscopic interaction with an electromagnetic field. The GSTCs allow this surface distribution of scatterers to be replaced with a boundary condition that is applied across an infinitely thin equivalent surface (hence the name metasurface, metafilm, or metascreen), as indicated in Fig. 1.17. The size, shape, and spacing of the scatterers are incorporated into this boundary condition through the polarizability densities of the scatterers on the interface. These surface polarizability densities are related to the effective surface susceptibilities and surface porosities.

The GSTCs for a metasurface take on different forms for either a metafilm or a metascreen. For a metafilm the GSTCs apply to jumps in both the tangential compo-

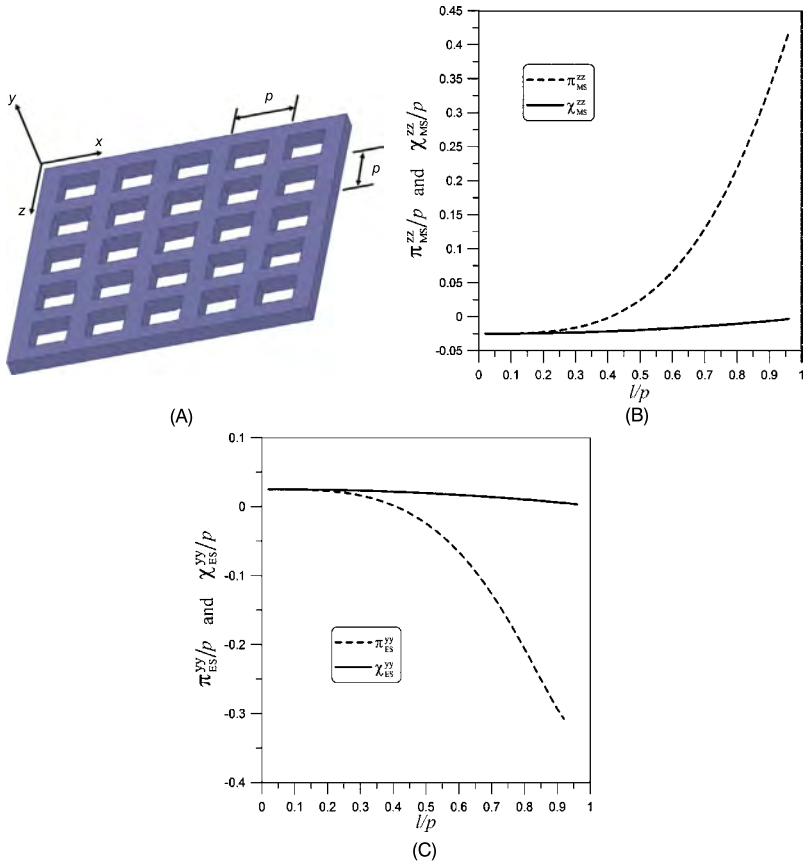

Figure 1.16 Surface susceptibilities and surface porosities for a metascreen composed of an array of square apertures of length l: (A) array of square apertures (from C.L. Holloway, E.F. Kuester, Generalized sheet transition conditions (GSTCs) for a metascreen, IEEE Trans. Antennas Propag. 66 (5) (2018) 2414–2427, © 2018 IEEE), (B) χ_{MS}^{zz} and π_{MS}^{zz} for square apertures ($h = 5$ mm and $p = 100$ mm), and (C) χ_{ES}^{yy} and π_{ES}^{yy} for circular apertures ($h = 5$ mm and $p = 100$ mm).

nents of the electric (E) and magnetic (H) fields across the metafilm [see Figs. 1.17A and 1.17C] and take on the following form [108,110,113]:

$$\mathbf{a}_y \times \left[\mathbf{E}^{\mathrm{A}} - \mathbf{E}^{\mathrm{B}}\right]_{y=0} = -j\omega\mu_0 \left(\overleftrightarrow{\boldsymbol{\chi}}_{MS} \cdot \tilde{\mathbf{H}}_{\mathrm{av}}\right)_t - \mathbf{a}_y \times \nabla_t \left(\mathbf{a}_y \cdot \overleftrightarrow{\boldsymbol{\chi}}_{ES} \cdot \tilde{\mathbf{E}}_{\mathrm{av}}\right) \quad (1.18)$$

and

$$\mathbf{a}_y \times \left[\mathbf{H}^{\mathrm{A}} - \mathbf{H}^{\mathrm{B}}\right]_{y=0} = j\omega\epsilon_0 \left(\overleftrightarrow{\boldsymbol{\chi}}_{ES} \cdot \tilde{\mathbf{E}}_{\mathrm{av}}\right)_t - \mathbf{a}_y \times \nabla_t \left(\mathbf{a}_y \cdot \overleftrightarrow{\boldsymbol{\chi}}_{MS} \cdot \tilde{\mathbf{H}}_{\mathrm{av}}\right), \quad (1.19)$$

where the average fields are defined by

$$\mathbf{E}_{\mathrm{av}} = \frac{1}{2}\left(\mathbf{E}^{\mathrm{A}} + \mathbf{E}^{\mathrm{B}}\right)_t + \frac{1}{2}\epsilon_0 \, \mathbf{a}_y \left(D_y^A + D_y^B\right), \quad (1.20)$$

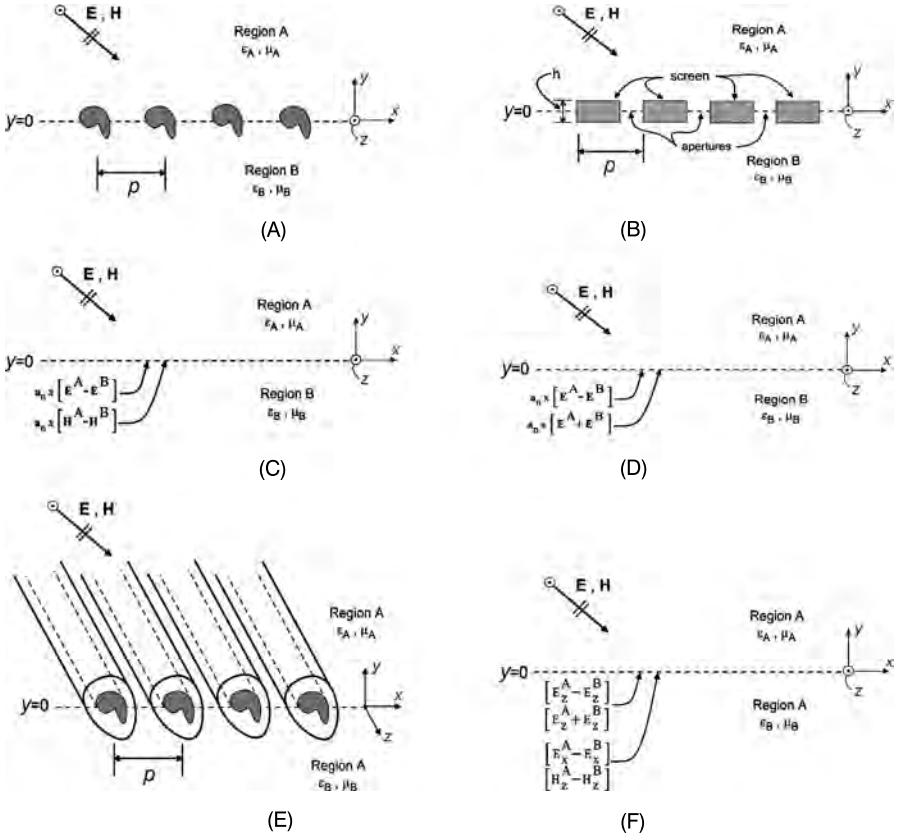

Figure 1.17 Reference plane to allow GSTCs: (A) a metafilm with arbitrarily shaped scatterers, (B) a metascreen with arbitrarily shaped apertures, (C) reference plane for a metafilm at which the GSTCs are applied, (D) reference plane for a metascreen at which the GSTCs are applied, (E) a metagrating with arbitrary shaped coated wire grating, and (F) reference plane for a metagrating at which the GSTCs are applied.

and similarly for $\mathbf{H}_{\text{av}}$, $\mathbf{D}_{\text{av}}$, and $\mathbf{B}_{\text{av}}$. The surface susceptibility dyadics are defined as

$$\begin{aligned}\overleftrightarrow{\chi}_{ES} = {} & \chi_{ES}^{xx}\mathbf{a}_x\mathbf{a}_x + \chi_{ES}^{xy}\mathbf{a}_x\mathbf{a}_y + \chi_{ES}^{xz}\mathbf{a}_x\mathbf{a}_z \\ & + \chi_{ES}^{yx}\mathbf{a}_y\mathbf{a}_x + \chi_{ES}^{yy}\mathbf{a}_y\mathbf{a}_y + \chi_{ES}^{yz}\mathbf{a}_y\mathbf{a}_z \\ & + \chi_{ES}^{zx}\mathbf{a}_x\mathbf{a}_x + \chi_{ES}^{zy}\mathbf{a}_z\mathbf{a}_y + \chi_{ES}^{zz}\mathbf{a}_z\mathbf{a}_z\,, \end{aligned} \tag{1.21}$$

$$\begin{aligned}\overleftrightarrow{\chi}_{MS} = {} & \chi_{MS}^{xx}\mathbf{a}_x\mathbf{a}_x + \chi_{MS}^{xy}\mathbf{a}_x\mathbf{a}_y + \chi_{MS}^{xz}\mathbf{a}_x\mathbf{a}_z \\ & + \chi_{MS}^{yx}\mathbf{a}_y\mathbf{a}_x + \chi_{MS}^{yy}\mathbf{a}_y\mathbf{a}_y + \chi_{MS}^{yz}\mathbf{a}_y\mathbf{a}_z \\ & + \chi_{MS}^{zx}\mathbf{a}_x\mathbf{a}_x + \chi_{MS}^{zy}\mathbf{a}_z\mathbf{a}_y + \chi_{MS}^{zz}\mathbf{a}_z\mathbf{a}_z\,. \end{aligned} \tag{1.22}$$

The surface susceptibilities have units of length.

For a metascreen, a different set of GSTCs is needed. For a metascreen, a boundary condition for the magnetic field is not usable *a priori*, because it would involve surface currents that are not yet known, much like what occurs for a wire grating [112]. The required GSTCs for a metascreen should constrain only tangential E [see Figs. 1.17B and 1.17D], and can be expressed as conditions on the jump of the tangential E-field and on the sum (twice the average) of the tangential E-fields [33,109]:

$$\begin{aligned}\mathbf{a}_y \times \left[\mathbf{E}^{\mathrm{A}}(\mathbf{r}_o) - \mathbf{E}^{\mathrm{B}}(\mathbf{r}_0)\right] = &- \mathbf{a}_x\, j\omega\mu_0 \left[\chi_{MS}^{Axx} H_x^A(\mathbf{r}_o) + \chi_{MS}^{Bxx} H_x^B(\mathbf{r}_o)\right. \\ &\left. + \chi_{MS}^{Axz} H_z^A(\mathbf{r}_o) + \chi_{MS}^{Bxz} H_z^B(\mathbf{r}_o)\right] \\ &- \mathbf{a}_z\, j\omega\mu_0 \left[\chi_{MS}^{Azx} H_x^A(\mathbf{r}_o) + \chi_{MS}^{Bzx} H_x^B(\mathbf{r}_o)\right. \\ &\left. + \chi_{MS}^{Azz} H_z^A(\mathbf{r}_o) + \chi_{MS}^{Bzz} H_z^B(\mathbf{r}_o)\right] \\ &- \mathbf{a}_y \times \left[\chi_{ES}^{Ayy} \nabla_t E_y^A(\mathbf{r}_o) + \chi_{ES}^{Byy} \nabla_t E_y^B(\mathbf{r}_o)\right]\end{aligned} \tag{1.23}$$

and

$$\begin{aligned}\mathbf{a}_y \times \left[\mathbf{E}^{\mathrm{A}}(\mathbf{r}_o) + \mathbf{E}^{\mathrm{B}}(\mathbf{r}_0)\right] = &- \mathbf{a}_x\, j\omega\mu_0 \left[\pi_{MS}^{Axx} H_x^A(\mathbf{r}_o) - \pi_{MS}^{Bxx} H_x^B(\mathbf{r}_o)\right. \\ &\left. + \pi_{MS}^{Axz} H_z^A(\mathbf{r}_o) - \pi_{MS}^{Bxz} H_z^B(\mathbf{r}_o)\right] \\ &- \mathbf{a}_z\, j\omega\mu_0 \left[\pi_{MS}^{Azx} H_x^A(\mathbf{r}_o) - \pi_{MS}^{Bzx} H_x^B(\mathbf{r}_o)\right. \\ &\left. + \pi_{MS}^{Azz} H_z^A(\mathbf{r}_o) - \pi_{MS}^{Bzz} H_z^B(\mathbf{r}_o)\right] \\ &- \mathbf{a}_y \times \left[\pi_{ES}^{Ayy} \nabla_t E_y^A(\mathbf{r}_o) - \pi_{ES}^{Byy} \nabla_t E_y^B(\mathbf{r}_o)\right].\end{aligned} \tag{1.24}$$

As before, χ_{ES} and χ_{MS} are interpreted as effective electric and magnetic surface susceptibilities, respectively, while π_{ES} and π_{MS} are interpreted as effective electric and magnetic surface porosities of the metascreen [109]. Like the surface susceptibilities, the surface porosities have units of length.

A metagrating [112] behaves like a metafilm to electric fields perpendicular to the wire axes, but like a metascreen for electric fields parallel to the wire axes [see Figs. 1.17E and 1.17F]. Metagratings require GSTCs that are a combination of those needed for a metafilm and a metascreen, which are given by the following:

$$\begin{aligned}\mathbf{a}_y \times \left[\mathbf{E}^{A}(\mathbf{r}_o) - \mathbf{E}^{B}(\mathbf{r}_o)\right] = &- j\omega\mu_0\, \chi_{MS}^{zz} H_{z,av}(\mathbf{r}_o)\, \mathbf{a}_z - j\omega\, \chi_{MS}^{xy} B_{y,av}(\mathbf{r}_o)\, \mathbf{a}_x \\ &- j\omega \left[\chi_{MS}^{Axx}\, B_x^A(\mathbf{r}_o) + \chi_{MS}^{Bxx}\, B_x^B(\mathbf{r}_o)\right] \mathbf{a}_x \\ &- \mathbf{a}_y \times \left[\chi_{ES}^{yx} \nabla E_{x,av}(\mathbf{r}_o)\right] \\ &- \mathbf{a}_y \times \left[\chi_{ES}^{Ayy} \nabla E_y^A(\mathbf{r}_o) + \chi_{ES}^{Byy} \nabla E_y^B(\mathbf{r}_o)\right],\end{aligned} \tag{1.25}$$

$$
\begin{aligned}
H_z^A(\mathbf{r}_o) - H_z^B(\mathbf{r}_o) = {} & j\omega\epsilon_0\, \chi_{ES}^{xx}\, E_{x,av}(\mathbf{r}_o) \\
& + j\omega\epsilon_0 \left[\chi_{ES}^{Axy}\, E_y^A(\mathbf{r}_o) + \chi_{ES}^{Bxy}\, E_y^B(\mathbf{r}_o) \right] \\
& - \frac{1}{\mu_0} \left[\chi_{MS}^{yy}\, \frac{\partial B_{y,av}(\mathbf{r}_o)}{\partial z} + \chi_{MS}^{Ayx}\, \frac{\partial B_x^A(\mathbf{r}_o))}{\partial z} \right. \\
& \left. + \chi_{MS}^{Byx}\, \frac{\partial B_x^B(\mathbf{r}_o)}{\partial z} \right],
\end{aligned} \tag{1.26}
$$

and

$$
\begin{aligned}
E_z^A(\mathbf{r}_o) + E_z^B(\mathbf{r}_o) = {} & - j\omega\pi_{MS}^{xy} B_{y,av}(\mathbf{r}_o) \\
& - j\omega \left[\pi_{MS}^{Axx}\, B_x^A(\mathbf{r}_o) - \pi_{MS}^{Bxx}\, B_x^B(\mathbf{r}_o) \right] \\
& - \pi_{ES}^{xy} \frac{\partial E_{x,av}(\mathbf{r}_o)}{\partial z} - \pi_{ES}^{Ayy} \frac{\partial E_y^A(\mathbf{r}_o)}{\partial z} \\
& - \pi_{ES}^{Byy} \frac{\partial E_y^B(\mathbf{r}_o)}{\partial z}.
\end{aligned} \tag{1.27}
$$

The coefficients χ_{ES} and χ_{MS} are effective electric and magnetic surface susceptibilities of the metagrating, while π_{ES} and π_{MS} are effective electric and magnetic surface *porosities* of the metagrating; both have units of length.

Calculating the surface susceptibilities and surface porosities can be difficult for generally-shaped inclusions or apertures. However, the GSTCs can be used to retrieve these surface parameters from measured or calculated plane-wave reflection and transmission coefficients, as done in [33,113,114], and [117–119]. These GSTCs, along with the surface parameters, are also convenient to use in the analysis of various applications of the EM interaction of metasurfaces with EM fields [47,111,115–123].

The GSTCs can also be cast in the form of impedance-type boundary conditions [13,160–163]. For plane-wave fields, whose variation parallel to a metafilm is of the form

$$
e^{-j\mathbf{k}\cdot\mathbf{r}_t}, \tag{1.28}
$$

where

$$
\mathbf{k} = k_x \mathbf{a}_x + k_y \mathbf{a}_y \quad \text{and} \quad \mathbf{r}_t = x\mathbf{a}_x + y\mathbf{a}_y, \tag{1.29}
$$

we can use Maxwell's equations to write Eqs. (1.18) and (1.19) as

$$
\mathbf{a}_y \times \left[\mathbf{E}^{\mathrm{A}} - \mathbf{E}^{\mathrm{B}} \right]_{y=0} = - \overleftrightarrow{\mathbf{Z}}_{MS} \cdot \mathbf{H}_{t,av}, \tag{1.30}
$$

$$
\mathbf{a}_y \times \left[\mathbf{H}^{\mathrm{A}} - \mathbf{H}^{\mathrm{B}} \right]_{y=0} = \overleftrightarrow{\mathbf{Y}}_{ES} \cdot \mathbf{E}_{t,av}. \tag{1.31}
$$

Here, the spatially dispersive (**k**-dependent) surface transfer admittance and transfer impedance are given by

$$\overleftrightarrow{Y}_{ES} = j\omega\overleftrightarrow{\chi}_{ES} + \frac{j\overleftrightarrow{\chi}_{MS}}{\omega\mu}(\mathbf{a}_z \times \mathbf{k})(\mathbf{a}_z \times \mathbf{k})\,, \tag{1.32}$$

$$\overleftrightarrow{Z}_{MS} = j\omega\overleftrightarrow{\chi}_{MS} + \frac{j\overleftrightarrow{\chi}_{ES}}{\omega\epsilon}(\mathbf{a}_z \times \mathbf{k})(\mathbf{a}_z \times \mathbf{k})\,. \tag{1.33}$$

Boundary conditions of this form can also be interpreted as lumped elements in equivalent transmission-line circuits [161].

1.5 Isolated scatterers and one-dimensional array

So far we have discussed three-dimensional metamaterials and two-dimensional metasurfaces. What about one-dimensional metastructures? The two-dimensional metamaterial (i.e., a metasurface) concept can be extended even further to the concept of using only a linear unit cell rather than a surface cell, that is, using only a single subwavelength resonant structure for some desired effect or behavior. In fact, we have already begun to see a few applications of this concept. One in particular is the use of a unit cell in the design of electrically small antennas. In antenna applications, the unit cell acts like a parasitic element to the radiating element of the antenna and serves as a means to match the electrically small radiating element to both (1) the feeding transmission line and (2) free space. Such designs have been shown to achieve efficient electrically small antennas [164–171]. Nanoparticles have also been used for tuning "so-called" optical nanoantennas [172]. An additional example is the use of a one-dimensional unit cell as a tuning structure for planar transmission lines [173]. Another emerging area of application is the use of one-dimensional chains of nanoparticles as waveguides supporting surface waves, of which examples can be found in [174–180].

1.6 Summary

The recent development of various engineered materials (3-D metamaterials, 2-D metasurfaces, single arrays and single particles) is bringing us closer to realizing the exciting predictions (exotic material behavior) made over one hundred years ago by the work of Lamb, Schuster, and Pocklington [60–62]. As we saw from the many references cited in this chapter, in recent years, many authors have studied the properties and potential applications of these exotic materials. While there is still much work needed in the understanding, analysis, design, and fabrication of these engineered materials, the potential of these materials has forever changed the landscape of RF, microwaves, optics and photonics for the future. This book intends to address some of the potential applications of these engineered materials. Including this chapter, the book contains a total of 9 chapters covering different aspects of dielectric metastruc-

tures (i.e., metamaterials, metasurfaces, isolated scatterers, and one-dimensional linear arrays).

References

[1] A. Fresnel, La loi des modifications que la réflexion imprime à la lumière polarisée, Mem. Acad. R. Sci. Inst. France 11 (1832) 393–433.

[2] J.C. Maxwell, A Treatise on Electricity and Magnetism, Vol. 1, Dover, New York, 1954, sections 306–307.

[3] Lord Rayleigh, On the influence of obstacles arranged in rectangular order on the properties of a medium, Philos. Mag. Ser. 5 34 (1892) 481–502.

[4] M. Born, E. Wolf, Principles of Optics: Electromagnetic Theory of Propagation, Interference and Diffraction of Light, sixth ed., Pergamon Press, Oxford, 1980.

[5] S. Zouhdi, A. Sihvola, M. Arsalane (Eds.), Advances in Electromagnetics of Complex Media and Metamaterials, Kluwer Academic Pub., Boston, 2002.

[6] C. Caloz, T. Itoh, Electromagnetic Metamaterials: Transmission Line Theory and Microwave Applications, Wiley–IEEE Press, 2005.

[7] G.V. Eleftheriades, K.G. Balmain, Negative Refraction Metamaterials: Fundamental Principles and Applications, Wiley, 2005.

[8] N. Engheta, R.W. Ziolkowski, Electromagnetic Metamaterials: Physics and Engineering Explorations, John Wiley & Sons, 2006.

[9] R. Marqués, F. Martín, M. Sorolla, Metamaterials With Negative Parameters: Theory, Design, and Microwave Applications, Wiley–Interscience, Hoboken, NJ, 2008.

[10] F. Capolino (Ed.), Metamaterials Handbook: Theory and Phenomena of Metamaterials, CRC Press, Boca Raton, FL, 2009.

[11] T.J. Cui, D.R. Smith, R. Liu (Eds.), Metamaterials: Theory, Design, and Applications, Springer, New York, 2010.

[12] V.G. Veselago, The electrodynamics of substances with simultaneously negative values of ϵ and μ, Usp. Fiz. Nauk 92 (1967) 517–526 [in Russian], Engl. transl. in Sov. Phys. Usp. 10 (1968) 509–514.

[13] S. Tretyakov, Analytical Modeling in Applied Electromagnetics, Artech House, Boston, 2003.

[14] A. Sihvola, Metamaterials in electromagnetics, Metamaterials 1 (1) (2007) 2–11.

[15] E. Shamonina, L. Solymar, Metamaterials: how the subject started, Metamaterials 1 (1) (2007) 12–18.

[16] M. Lapine, S. Tretyakov, Contemporary notes on metamaterials, IET Microw. Antennas Propag. 1 (1) (2007) 3–11.

[17] J.B. Pendry, A.J. Holden, W.J. Stewart, I. Youngs, Extremely low frequency plasmons in metallic mesostructure, Phys. Rev. Lett. 76 (1996) 4773–4776.

[18] J.B. Pendry, A.J. Holden, D.J. Robbins, W.J. Stewart, Magnetism from conductors and enhanced nonlinear phenomena, IEEE Trans. Microw. Theory Tech. 47 (1999) 2075–2084.

[19] C.A. Kyriazidou, H.F. Contopanagos, W.M. Merrill, N.G. Alexópoulos, Artificial versus natural crystals: effective wave impedance of printed photonic bandgap materials, IEEE Trans. Antennas Propag. 48 (2000) 95–105.

[20] C.A. Kyriazidou, R.E. Daiz, N.G. Alexópoulos, Novel material with narrow-band transparency window in the bulk, IEEE Trans. Antennas Propag. 48 (2000) 107–116.

[21] D.R. Smith, D.C. Vier, N. Kroll, S. Schultz, Direct calculation of permeability and permittivity for a left-handed metamaterial, Appl. Phys. Lett. 77 (2000) 2246–2248.
[22] S.G. Johnson, J.D. Joannopoulos, Three-dimensionally periodic dielectric layered structure with omnidirectional photonic band gap, Appl. Phys. Lett. 77 (2000) 3490–3492.
[23] P. Markos, C.M. Soukoulis, Numerical studies of left-handed materials and arrays of split ring resonators, Phys. Rev. E 65 (2002) 036622-1–036622-8.
[24] N. Engheta, S.R. Nelatury, A. Hoorfar, Omega media as a metamaterial with negative permittivity and permeability, in: Dig. of USNC/URSI Meeting, San Antonio, TX, June 16–21, 2002, p. 47.
[25] J.B. Pendry, A.J. Holden, D.J. Robbins, W.J. Stewart, Extremely low frequency plasmons in thin-wire structures, J. Phys. Condens. Matter 10 (1998) 4785–4809.
[26] D.A. Smith, N. Kroll, Negative refractive index in left-handed materials, Phys. Rev. Lett. 85 (2000) 2933–2936.
[27] D.R. Smith, W.J. Padilla, D.C. Vier, S.C. Nemat-Nasser, S. Schultz, Composite medium with simultaneously negative permeability and permittivity, Phys. Rev. Lett. 84 (2000) 4184–4186.
[28] R. Marques, J. Martel, F. Mesa, F. Medina, A new 2D isotropic left-handed metamaterial design: theory and experiment, Microw. Opt. Technol. Lett. 35 (5) (2002) 405–408.
[29] C.L. Holloway, E.F. Kuester, J. Baker-Jarvis, P. Kabos, A double negative (DNG) composite medium composed of magneto-dielectric spherical particles embedded in a matrix, IEEE Trans. Antennas Propag. 51 (10) (2003) 2596–2603.
[30] E.F. Kuester, N. Memić, S. Shen, A.D. Scher, S. Kim, K. Kumley, H. Loui, A negative refractive index metamaterial based on a cube array of layered nonmagnetic spherical particles, Prog. Electromagn. Res. B 33 (2011) 175–202.
[31] R.W. Ziolkowski, E. Heyman, Wave propagation in media having negative permittivity and permeability, Phys. Rev. E 64 (2001) 056625.
[32] R.A. Shelby, D.R. Smith, S.C. Nemat-Nasser, S. Schultz, Microwave transmission through a two-dimensional, isotropic left-handed material, Appl. Phys. Lett. 78 (2001) 489–491.
[33] C.L. Holloway, E.F. Kuester, J.A. Gordon, J. O'Hara, J. Booth, D.R. Smith, An overview of the theory and applications of metasurfaces: the two-dimensional equivalents of metamaterials, IEEE Antennas Propag. Mag. 54 (2) (April 2012) 10–35.
[34] A.A. Maradudin (Ed.), Structured Surfaces as Optical Metamaterials, Cambridge University Press, Cambridge, UK, 2011.
[35] J.D. Jackson, Classical Electrodynamics, Wiley, New York, 1999.
[36] P.S. Neelakanta, Handbook of Electromagnetic Materials, CRC Press, New York, 1995.
[37] A.H. Sihvola, Electromagnetic Mixing Formulas and Application, The Institution of Electrical Engineers, London, United Kingdom, 1999.
[38] L. Lewin, The electrical constants of a material loaded with spherical particles, Proc. Inst. Elec. Engrs. 94 (part 3) (1947) 65–68.
[39] R. Gans, H. Happel, Zur Optik kolloidaler Metallösungen, Ann. Phys. 29 (1909) 277–300.
[40] J.A. Stratton, The effect of rain and fog on the propagation of very short radio waves, Proc. IRE 18 (1930) 1064–1074.
[41] E.F. Kuester, C.L. Holloway, Comparison of approximations for effective parameters of artificial dielectrics, IEEE Trans. Microw. Theory Tech. 38 (1990) 1752–1755.
[42] W. Rotman, Plasma simulation by artificial dielectrics and parallel-plate media, IRE Trans. Antennas Propag. 10 (1962) 82–95.
[43] N.A. Khizhniak, Artificial anisotropic dielectrics: I, Zh. Tekh. Fiz. 27 (1957) 2006–2013, [in Russian], Engl. transl. in Sov. Phys. Tech. Phys. 2 (1957) 1858–1864.

[44] N.A. Khizhniak, Artificial anisotropic dielectrics: II, Zh. Tekh. Fiz. 27 (1957) 2014–2026 [in Russian], Engl. transl. in Sov. Phys. Tech. Phys. 2 (1957) 1865–1876.
[45] N.A. Khizhniak, Artificial anisotropic dielectrics: III, Zh. Tekh. Fiz. 27 (1957) 2027–2037 [in Russian], Engl. transl. in Sov. Phys. Tech. Phys. 2 (1957) 1877–1886.
[46] R.E. Collin, Field Theory of Guided Waves, IEEE Press, New York, 1991, Chap. 12.
[47] C.L. Holloway, E.F. Kuester, Corrections to the classical continuity conditions at the interface of a composite medium, Photonics Nanostruct. Fundam. Appl. 11 (4) (November 2013) 397–422.
[48] R.N. Bracewell, Analogues of an ionized medium, Wirel. Eng. 31 (1954) 320–326.
[49] E.F. Kuester, C.L. Holloway, A low-frequency model for wedge or pyramid absorber array – I: theory, IEEE Trans. Electromagn. Compat. 36 (4) (1994) 300–306.
[50] M. Johansson, C.L. Holloway, E.F. Kuester, Effective electromagnetic properties of honeycomb composites, and hollow pyramidal and alternating wedge absorbers, IEEE Trans. Antennas Propag. 53 (2) (Feb 2005) 728–736.
[51] Z. Hashin, S. Shtrikman, A variational approach to the theory of the effective magnetic permeability of multiphase materials, J. Appl. Phys. 33 (1962) 3125–3131.
[52] K. Lichtenecker, Über den widerstand gewisser zusammengesetzter körperlicher Leiter, Phys. Z. 19 (1918) 374–382.
[53] K. Lichtenecker, Der elektrische leitungswiderstand künstlicher und natürlicher Aggregate, Phys. Z. 25 (1924) 169–181, 193–204, 225–233.
[54] L. Brillouin, Wave Propagation in Periodic Structures, Dover Pub., New York, 1953, Chapter 7.
[55] A. Ishimaru, Electromagnetic Wave Propagation, Radiation, and Scattering, Prentice Hall, Englewood Cliffs, N.J., 1991, Chapter 7.
[56] J.A. Kong, Electromagnetic Wave Theory, John Wiley & Sons, N.Y., 1986, Chapter 6.
[57] T.K. Wu, Frequency Selective Surface and Grid Array. , John Wiley & Sons, Inc., N.Y., 1995.
[58] B.A. Munk, Frequency Selective Surfaces: Theory and Design, Wiley, Inc., 2000.
[59] C.M. Soukoulis, Photonic Band Gap Materials, Kluwer Academic Publishers, Dordrecht, 1996.
[60] H. Lamb, On group-velocity, Proc. Lond. Math. Soc., Ser. 2 1 (1904) 473–479.
[61] A. Schuster, An Introduction to the Theory of Optics, Edward Arnold, London, 1904, pp. 313–318.
[62] H.C. Pocklington, Growth of a wave-group when the group velocity is negative, Nature 71 (1905) 607–608.
[63] L.I. Mandel'shtam, Lectures on certain problems of oscillation theory: Lecture 4, in: Polnoe Sobraniye Trudov, tom 5, Izdat. Akad. Nauk SSSR, Leningrad, 1950, pp. 461–467 [in Russian], also in his Lektsii po Optike, Teorii Otnositel'nosti i Kvantovoi Mekhanike, Nauka, Moscow, 1972, pp. 431–437.
[64] L.I. Mandel'shtam, Group velocity in crystalline arrays, Zh. Eksp. Teor. Fiz. 15 (1945) 475–478 [in Russian], also in: Polnoe Sobraniye Trudov, tom 2, Izdat. Akad. Nauk SSSR, Leningrad, 1945, pp. 334–338.
[65] G.D. Malyuzhinets, A note on the radiation principle, Zh. Tekh. Fiz. 21 (1951) 940–942 [in Russian].
[66] D.V. Sivukhin, The energy of electromagnetic fields in dispersive media, Opt. Spektrosk. 3 (1957) 308–312 [in Russian].
[67] E. Shamonina, Slow waves in magnetic metamaterials: history, fundamentals and applications, Phys. Status Solidi B 245 (2008) 1471–1482.

[68] R.A. Silin, On the history of backward electromagnetic waves in metamaterials, Metamaterials 6 (2012) 1–7.
[69] S.A. Tretyakov, A personal view on the origins and developments of the metamaterial concept, J. Opt. 19 (2017) 013002.
[70] P. Markoš, C.M. Soukoulis, Transmission studies of left-handed materials, Phys. Rev. B 65 (2001) 033401.
[71] R.M. Walser, A.P. Valanju, P.M. Valanju, Comment on: extremely low frequency plasmons in metallic mesostructures, Phys. Rev. Lett. 87 (2001) 119701.
[72] I.V. Lindell, S.A. Tretyakov, K.I. Nikoskinen, S. Iivonen, BW media-media with negative parameters, capable of supporting backward waves, Microw. Opt. Technol. Lett. 31 (2001) 129–133.
[73] S.A. Tretyakov, Meta-material with wideband negative permittivity and permeability, Microw. Opt. Technol. Lett. 31 (2001) 163–165.
[74] C. Caloz, C.-C. Chang, T. Itoh, Full-wave verification of the fundamental properties of left-handed materials in waveguide configurations, J. Appl. Phys. 90 (2001) 5483–5486.
[75] R.A. Silin, I.P. Chepurnykh, On media with negative dispersion, Radiotekh. Elektron. 46 (2001) 1212–1217 [in Russian], Engl. transl. in J. Commun. Technol. Electron. 46 (2001) 1121–1125.
[76] P.M. Valanju, R.M. Walser, A.P. Valanju, Wave refraction in negative-index media: always positive and very inhomogeneous, Phys. Rev. Lett. 88 (2002) 187401-1–187401-4.
[77] O.G. Vendik, M.S. Gasinova, Artificial double negative (DNG) media composed by two different dielectric sphere lattices embedded in a dielectric matrix, in: 34th European Microwave Conference, Amsterdam, 2004, pp. 1209–1212.
[78] L. Jylha, I. Kolmakov, S. Maslovski, S. Tretyakov, Modeling of isotropic backward-wave materials composed of resonant spheres, J. Appl. Phys. 99 (2006) 043102.
[79] M.S. Wheeler, J.S. Aitchison, M. Mojahedi, Coated nonmagnetic spheres with a negative index of refraction at infrared frequencies, Phys. Rev. B 73 (2006) 045105.
[80] Q. Zhao, J. Zhou, F. Zhang, D. Lippens, Mie resonance-based dielectric metamaterials, Mater. Today 12 (12) (Dec. 2009) 60–69.
[81] L. Peng, L. Ran, H. Chen, H. Zhang, J. auKong, T.M. Grzegorczyk, Experimental observation of left-handed behavior in an array of standard dielectric resonators, Phys. Rev. Lett. 98 (2007) 157403.
[82] J. Kim, A. Gopinath, Simulation of a metamaterial containing cubic high dielectric resonators, Phys. Rev. B 76 (2007) 115126.
[83] Q. Zhao, L. Kang, B. Du, H. Zhao, Q. Xie, X. Huang, B. Li, J. Zhou, L. Li, Experimental demonstration of isotropic negative permeability in a three-dimensional dielectric composite, Phys. Rev. Lett. 101 (July 2008) 027402.
[84] S. Kim, C.L. Holloway, K.L. Kumley, M.D. Janezic, J. Baker-Jarvis, E.F. Kuester, A frequency-bandgap waveguide controlled with metafilms composed of cubic particles, J. Appl. Phys. 112 (2012) 104904.
[85] P. Moitra, B.A. Slovick, W. Li, I.I. Kravchencko, D.P. Briggs, S. Krishnamurthy, J. Valentine, Large-scale all-dielectric metamaterial perfect reflectors, ACS Photonics 2 (6) (2015) 692–698.
[86] J.C. Ginn, G.A. Ten Eyck, I. Brener, D.W. Peters, M.B. Sinclair, Infrared cubic dielectric resonator metamaterial, in: Photonic Metamaterials and Plasmonics, Tucson, Arizona, June 7–8, 2010.
[87] J.C. Ginn, I. Brener, D.W. Peters, J.R. Wendt, J.O. Stevens, P.F. Hines, L.I. Basilio, Larry K. Warne, Jon F. Ihlefeld, Paul G. Clem, Michael B. Sinclair, Realizing optical magnetism from dielectric metamaterials, Phys. Rev. Lett. 108 (2012) 097402.

[88] I. Staude, A.E. Miroshnichenko, M. Decker, N.T. Fofang, S. Liu, E. Gonzales, J. Dominguez, T. Shan Luk, D.N. Neshev, I. Brener, Y. Kivshar, Tailoring directional scattering through magnetic and electric resonances in subwavelength silicon nanodisks, ACS Nano 7 (9) (2013) 7824–7832.

[89] S. Liu, M.B. Sinclair, S. Saravi, G.A. Keeler, Y. Yang, J. Reno, G.M. Peake, F. Setzpfandt, I. Staude, T. Pertsch, I. Brener, Resonantly enhanced second-harmonic generation using III–V semiconductor all-dielectric metasurfaces, Nano Lett. 16 (9) (2016) 5426–5432.

[90] I. Staude, V.V. Khardikov, N.T. Fofang, S. Liu, M. Decker, D.N. Neshev, T. Shan Luk, I. Brener, Y.S. Kivshar, Shaping photoluminescence spectra with magnetoelectric resonances in all-dielectric nanoparticles, ACS Photonics 2 (2) (2015) 172–177.

[91] S. Liu, G.A. Keeler, J.L. Reno, M.B. Sinclair, I. Brener, III–V semiconductor nanoresonators—a new strategy for passive, active, and nonlinear all-dielectric metamaterials, Adv. Opt. Mater. 4 (10) (2016) 1457.

[92] I. Brener, Optical magnetism from dielectric resonator metamaterials, in: META 2014 Conference, Singapore, May 20–23, 2014.

[93] L.K. Warne, L.I. Basilio, W.L. Langston, W.A. Johnson, M.B. Sinclair, Perturbation theory in the design of degenerate rectangular dielectric resonators, PIER B 44 (2012) 1–29.

[94] L.K. Warne, L.I. Basilio, W.L. Langston, W.A. Johnson, M.B. Sinclair, Perturbation theory in the design of degenerate spherical dielectric resonators, IEEE Trans. Antennas Propag. 61 (2013) 2130–2141.

[95] L.K. Warne, W.A. Johnson, L.I. Basilio, W.L. Langston, M.B. Sinclair, Subcell method for modeling metallic resonators in metamaterials, PIER B 38 (2012) 135–164.

[96] A.M. Nicolson, G. Ross, Measurement of the intrinsic properties of materials by time domain techniques, IEEE Trans. Instrum. Meas. 19 (1970) 377–382.

[97] W.B. Weir, Automatic measurements of complex dielectric constant and permeability at microwave frequencies, Proc. IEEE 62 (1974) 33–36.

[98] D.R. Smith, S. Schultz, P. Markos, C.M. Soukoulis, Determination of effective permittivity and permeability of metamaterials from reflection and transmission coefficients, Phys. Rev. B 65 (2002) 195104.

[99] R.W. Ziolkowski, Designs, fabrication, and testing of double negative metamaterials, IEEE Trans. Antennas Propag. 51 (2003) 1516–1529.

[100] S. Kim, E.F. Kuester, C.L. Holloway, A.D. Scher, J. Baker-Jarvis, Boundary effects on the determination of the effective parameters of a metamaterials from normal incidence reflection and transmissions, IEEE Trans. Antennas Propag. 59 (6) (2011).

[101] S. Kim, E.F. Kuester, C.L. Holloway, A.D. Scher, J. Baker-Jarvis, Effective material property extraction of a metamaterial by taking boundary effects into account at TE/TM polarized incidence, Prog. Electromag. Res. B 36 (2011) 1–33.

[102] X. Chen, T.M. Grezegorczyk, B.-I. Wu, J. Pacheco, J.A. Kong, Robust method to retrieve the constitutive effective parameters of metamaterials, Phys. Rev. E 70 (2004) 016608.

[103] A.D. Scher, E.F. Kuester, Extracting the bulk effective parameters of a metamaterial via the scattering parameters for a single planar array of particles, Metamaterials 3 (2009) 44–55.

[104] J. Zhou, T. Koschny, M. Kafesaki, C.M. Soukoulis, Size dependence and convergence of the retrieval parameters of metamaterials, Photonics Nanostruct. Fundam. Appl. 6 (2008) 96–101.

[105] C. Rockstuhl, T. Paul, F. Lederer, T. Pertsch, T. Zentgraf, T.P. Meyrath, H. Giessen, Transition from thin-film to bulk properties of metamaterials, Phys. Rev. B 77 (2008) 035126.

[106] C. Rockstuhl, C. Menzel, T. Paul, C. Helgert, E. Pshenay-Severin, J. Petschulat, A. Chipouline, T. Pertsch, F. Lederer, Bulk properties of metamaterials, Proc. SPIE 6987 (2008) 698710.
[107] M.G. Silveirinha, C.A. Fernandes, Homogenization of metamaterial surfaces and slabs: the crossed wire mesh canonical problem, IEEE Trans. Antennas Propag. 53 (2005) 59–69.
[108] C.L. Holloway, E.F. Kuester, A homogenization technique for obtaining generalized sheet transition conditions (GSTCs) for a metafilm embedded in a magneto-dielectric interface, IEEE Trans. Antennas Propag. 64 (11) (2016) 4671–4686.
[109] C.L. Holloway, E.F. Kuester, Generalized sheet transition conditions (GSTCs) for a metascreen, IEEE Trans. Antennas Propag. 66 (5) (2018) 2414–2427.
[110] E.F. Kuester, M.A. Mohamed, M. Piket-May, C.L. Holloway, Averaged transition conditions for electromagnetic fields at a metafilm, in: Special Issue on Metamaterials, IEEE Trans. Antennas Propag. 51 (10) (Oct. 2003) 2641–2651.
[111] C.L. Holloway, D.C. Love, E.F. Kuester, J.A. Gordon, D.A. Hill, Use of generalized sheet transition conditions to model guided waves on metasurfaces/metafilms, IEEE Trans. Antennas Propag. 60 (2012) 5173–5186.
[112] C.L. Holloway, E.F. Kuester, A homogenization technique for obtaining generalized sheet transition conditions for an arbitrarily shaped coated wire grating, Radio Sci. 49 (10) (2014) 813–850.
[113] C.L. Holloway, A. Dienstfrey, E.F. Kuester, J.F. O'Hara, A.K. Azad, A.J. Taylor, A discussion on the interpretation and characterization of metafilms–metasurfaces: the two-dimensional equivalent of metamaterials, Metamaterials 3 (2009) 100–112.
[114] C.L. Holloway, E.F. Kuester, A. Dienstfrey, Characterizing metasurfaces/metafilms: the connection between surface susceptibilities and effective material properties, IEEE Antennas Wirel. Propag. Lett. 10 (2011) 1507–1511.
[115] C.L. Holloway, M.A. Mohamed, E.F. Kuester, Reflection and transmission properties of a metafilm: with an application to a controllable surface composed of resonant particles, IEEE Trans. Electromagn. Compat. 47 (4) (Nov. 2005) 853–865.
[116] C.L. Holloway, D.C. Love, E.F. Kuester, A. Salandrino, N. Engheta, Sub-wavelength resonators: on the use of metafilms to overcome the $\lambda/2$ size limit, IET Microw. Antennas Propag. 2 (2) (March 2008) 120–129.
[117] C.L. Holloway, E.F. Kuester, Retrieval approach for determining surface susceptibilities and surface porosities of a symmetric metascreen from reflection and transmission coefficients, arXiv:1902.08703, 2019.
[118] C.L. Holloway, E.F. Kuester, A.H. Haddab, Using reflection and transmission coefficients to retrieve surface parameters for an anisotropic metascreen: with a discussion on conversion between TE and TM polarizations, J. Appl. Phys. 125 (2019) 095102.
[119] F. Yang, Y. Rahmat-Samii (Eds.), Surface Electromagnetics: With Applications in Antenna, Microwave, and Optical Engineering, Cambridge University Press, July 2019, Chapter 3: Using generalized sheet transition conditions (GSTCs) in the analysis of metasurfaces.
[120] C.L. Holloway, E.F. Kuester, D. Novotny, Waveguides composed of metafilms–metasurfaces: the two-dimensional equivalent of metamaterials, IEEE Antennas Wirel. Propag. Lett. 8 (2009) 525–529.
[121] C.L. Holloway, P. Kabos, M.A. Mohamed, E.F. Kuester, J. Gordon, M.D. Janezic, J. Baker-Jarvis, Realization of a controllable metafilm/metasurface composed of resonant magnetodielectric particles: measurements and theory, in: Special Issue on Microwave Metamaterials, IET Microw. Antennas Propag. 4 (8) (August 2010) 1111–1122.

[122] M.V. Rybin, D.S. Filonov, K.B. Samusev, P.A. Belov, Y.S. Kivshar, M.F. Limonov, Phase diagram for the transition from photonic crystals to dielectric metamaterials, Nat. Commun. 6 (1) (2015) 10102.

[123] J. Gordon, C.L. Holloway, J. Booth, Fluid interactions with metafilms/metasurfaces for tuning, sensing, and microwave-assisted chemical processes, Phys. Rev. B 83 (2011) 205130.

[124] S.A. Tretyakov, S.I. Maslovski, Thin absorbing structure for all incident angles based on the use of a high-impedance surface, Microw. Opt. Technol. Lett. 38 (3) (2003) 175–178.

[125] Y. Kotsuka, K. Murano, M. Amano, S. Sugiyama, Novel right-handed metamaterial based on the concept of 'autonomous control system of living cells,' and its absorber applications, IEEE Trans. Electromagn. Compat. 52 (3) (2010) 556–565.

[126] Hu Tao, C.M. Bingham, A.C. Strikwerda, D. Pilon, C. Shrekenhamer, N.I. Landy, K. Fan, X. Zhang, W.J. Padilla, R.D. Averitt, Highly flexible wide angle of incidence terahertz metamaterial absorber: design, fabrication, and characterization, Phys. Rev. B 78 (2008) 241103.

[127] N.I. Landy, S. Sajuyigbe, J.J. Mock, D.R. Smith, W.J. Padilla, Perfect metamaterial absorber, Phys. Rev. Lett. 100 (2008) 207402.

[128] O. Luukkonen, F. Costa, C.R. Simovski, A. Monorchio, S.A. Tretyakov, A thin electromagnetic absorber for wide incidence angles and both polarizations, IEEE Trans. Antennas Propag. 57 (10) (2009) 3119–3125.

[129] F. Bilotti, A. Toscano, K.B. Alici, E. Ozbay, L. Vegni, Design of miniaturized narrowband absorber based on resonant-magnetic inclusions, IEEE Trans. Electromagn. Compat. 53 (1) (2011) 63–72.

[130] S. Sajuyigbe, M. Ross, P. Geren, S.A. Cummer, M.H. Tanielian, D.R. Smith, Wide angle impedance matching metamaterials for waveguide-fed phased-array antenna, IET Microw. Antennas Propag. 4 (8) (2010) 1063–1072.

[131] H.-T. Chen, W.J. Padilla, J.M.O. Zide, S.R. Bank, A.C. Gossard, A.J. Taylor, R.D. Averitt, Ultrafast optical switching of terahertz metamaterials fabricated on ErAs/GaAs nanoisland superlattices, Opt. Lett. 32 (12) (2007) 1620–1622.

[132] H.-T. Chen, W.J. Padilla, J.M.O. Zide, A.C. Gossard, A.J. Taylor, R.D. Averitt, Active terahertz metamaterial devices, Nature 444 (2006) 597–600.

[133] H.-T. Chen, W.J. Padilla, M.J. Cich, A.K. Azad, R.D. Averitt, A.J. Taylor, A metamaterial solid-state terahertz phase modulator, Nat. Photonics 3 (2009) 148–151.

[134] H.-T. Chen, J.F. O'Hara, A.K. Azad, A.J. Taylor, R.D. Averitt, D.B. Shrekenhamer, W.J. Padilla, Experimental demonstration of frequency-agile terahertz metamaterials, Nat. Photonics 2 (2008) 295–298.

[135] W.L. Chan, H.-T. Chen, A.J. Taylor, I. Brener, M.J. Cich, D.M. Mittleman, A spatial light modulator for terahertz beams, Appl. Phys. Lett. 94 (2009) 213511.

[136] X.G. Peralta, I. Brener, W.J. Padilla, E.W. Young, A.J. Hoffman, M.J. Cich, R.D. Averitt, M.C. Wanke, J.B. Wright, H.-T. Chen, J.F. O'Hara, A.J. Taylor, J. Waldman, W.D. Goodhue, J. Li, J. Reno, External modulators for terahertz quantum-cascade lasers based on electrically-driven active metamaterials, Metamaterials 4 (2) (2010) 83–88.

[137] H. Tao, A.C. Strikwerda, K. Fan, W.J. Padilla, X. Zhang, R.D. Averitt, Reconfigurable terahertz metamaterials, Phys. Rev. Lett. 103 (2009) 147401.

[138] J. Han, A. Lakhtakia, Semiconductor split-ring resonators for thermally tunable terahertz metamaterials, J. Mod. Opt. 56 (2009) 554–557.

[139] T. Driscoll, S. Palit, M.M. Qazilbash, M. Brehm, F. Keilmann, B.-G. Chae, S.-J. Yun, H.-T. Kim, S.Y. Cho, N.M. Jokerst, D.R. Smith, D.N. Basov, Dynamic tuning of an

infrared hybrid-metamaterial resonance using vanadium dioxide, Appl. Phys. Lett. 93 (2008) 024101.
[140] T. Driscoll, H.-T. Kim, B.-G. Chae, B.-J. Kim, Y.-W. Lee, N.M. Jokerst, S. Palit, D.R. Smith, M. Di Ventra, D.N. Basov, Memory metamaterials, Science 325 (2009) 1518–1521.
[141] T. Driscoll, G.O. Andreev, D.N. Basov, S. Palit, S.Y. Cho, N.M. Jokerst, D.R. Smith, Tuned permeability in terahertz split-ring resonators for devices and sensors, Appl. Phys. Lett. 91 (2007) 062511.
[142] T.A. Klar, A.V. Kildishev, V.P. Drachev, V.M. Shalaev, Negative-index metamaterials: going optical, IEEE J. Sel. Top. Quantum Electron. 12 (6) (2006) 1106–1115.
[143] A.V. Kildishev, W. Cai, K. Chettiar, H. Yuan, A.K. Sarychev, V.P. Drachev, V.M. Shalaev, Negative refractive index in optics of metal-dielectric composites, J. Opt. Soc. Am. B 23 (3) (2006) 423–433.
[144] J.B. Pendry, Negative refraction makes a perfect lens, Phys. Rev. Lett. 85 (2000) 3966–3969.
[145] A. Alù, A. Salandrino, N. Engheta, Negative effective permeability and left-handed materials at optical frequencies, Opt. Express 14 (4) (2006) 1557–1567.
[146] G. Dolling, C. Enkrick, M. Wegener, C.M. Soukoulis, S. Linden, Low-loss negative-index metamaterials at telecommunication wavelengths, Opt. Lett. 31 (12) (2006) 1800–1802.
[147] T.J. Yen, W.J. Padilla, N. Fang, D.C. Vier, D.R. Smith, J.B. Pendry, D.N. Basov, X. Zhang, Terahertz magnetic response from artificial materials, Science 303 (2004) 1494–1496.
[148] J.A. Gordon, R.W. Ziolkowski, The design and simulated performance of a coated nanoparticle laser, Opt. Express 15 (5) (2007) 2622–2653.
[149] M.I. Stockman, Spasers explained, Nat. Photonics 2 (2008) 327–329.
[150] V.M. Shalaev, Optical negative-index metamaterials, Nat. Photonics 1 (2007) 41–48.
[151] A. Alu, N. Engheta, Theory of linear chains of metamaterials/plasmonic particles as subdiffraction optical nanotransmission lines, Phys. Rev. B 74 (2006) 205436.
[152] C. Pfeiffer, A. Grbic, Metamaterial Huygens' surfaces: tailoring wave fronts with reflectionless sheets, Phys. Rev. Lett. 110 (2013) 197401.
[153] C. Pfeiffer, A. Grbic, Cascaded metasurfaces for complete phase and polarization control, Appl. Phys. Lett. 102 (23) (2013) 231116.
[154] N.M. Estakhri, A. Alu, Wave-front transformation with gradient metasurfaces, Phys. Rev. X 6 (2016) 041008.
[155] A. Epstein, G.V. Eleftheriades, Arbitrary power-conserving field transformations with passive lossless omega-type bianisotropic metasurfaces, IEEE Trans. Antennas Propag. 64 (9) (2017).
[156] A.T. Pereda, F. Caminita, E. Martini, I. Ederra, J.C. Iriarte, R. Gonzalo, S. Maci, Dual circularly polarized broadside beam metasurface antenna, IEEE Trans. Antennas Propag. 64 (7) (2016) 2944–2953.
[157] S.B. Glybovski, S.A. Tretyakov, P.A. Belov, Y.S. Kivshar, C.R. Simovski, Metasurfaces: from microwaves to visible, Phys. Rep. 634 (2016) 1–72.
[158] D. Morits, M. Morits, V. Ovchinnikov, M. Omelyanovich, A. Tamminen, S. Tretyakov, C. Simovski, Multifunctional stretchable metasurface for the THz range, J. Opt. 16 (3) (2014) 032001.
[159] A. Alu, N. Engheta, Three-dimensional nanotransmission lines at optical frequencies: a recipe for broadband negative-refraction optical metamaterials, Phys. Rev. B 75 (2007) 024304.
[160] T.B.A. Senior, J.L. Volakis, Approximate Boundary Conditions in Electromagnetics, Stevenage, UK, IEE, 1995.

[161] M.I. Oksanen, S.A. Tretyakov, I.V. Lindell, Vector circuit theory for isotropic and chiral slabs, J. Electromagn. Waves Appl. 4 (1990) 613–643.
[162] S.A. Tretyakov, A.J. Viitanen, S.I. Maslovki, I.E. Saarela, Impedance boundary conditions for regular dense arrays of dipole scatterers, IEEE Trans. Antennas Propag. 51 (8) (2003) 2073–2078.
[163] O. Luukkonen, C. Simovski, G. Granet, G. Goussetis, D. Lioubtchenko, A.V. Räisänen, S.A. Tretyakov, Simple and accurate analytical model of planar grids and high-impedance surfaces comprising metal strips or patches, IEEE Trans. Antennas Propag. 56 (6) (2008) 1624–1632, correction in: IEEE Trans. Antennas Propag. 58 (2010) 2162.
[164] R.W. Ziolkowski, P. Jin, C.-C. Lin, Metamaterial-inspired engineering of antennas, Proc. IEEE 99 (10) (2011) 1720–1731.
[165] P. Jin, R.W. Ziolkowski, Metamaterial-inspired, electrically small, Huygens sources, IEEE Antennas Wirel. Propag. Lett. 9 (2010) 501–505.
[166] P. Jin, R.W. Ziolkowski, Multiband extensions of the electrically small metamaterial-engineered Z antenna, IET Microw. Antennas Propag. 4 (8) (2010) 1016–1025.
[167] C.-C. Lin, R.W. Ziolkowski, Dual-band 3D magnetic EZ antenna, Microw. Opt. Technol. Lett. 52 (4) (2010) 971–975.
[168] P. Jin, R.W. Ziolkowski, Broadband, efficient, electrically small metamaterial-inspired antennas facilitated by active near-field resonant parasitic elements, IEEE Trans. Antennas Propag. 58 (2) (2010) 318–327.
[169] P. Jin, R.W. Ziolkowski, Low Q, electrically small, efficient near field resonant parasitic antennas, IEEE Trans. Antennas Propag. 57 (9) (2009) 2548–2563.
[170] A. Erentok, R.W. Ziolkowski, Metamaterial-inspired efficient electrically-small antennas, IEEE Trans. Antennas Propag. 56 (3) (2008) 691–707.
[171] R.W. Ziolkowski, A. Erentok, Metamaterial-based efficient electrically small antennas, IEEE Trans. Antennas Propag. 54 (7) (2006) 2113–2130.
[172] A. Alu, N. Engheta, Tuning the scattering response of optical nanoantennas with nanocircuit loads, Nat. Photonics 2 (May 2008) 307–310.
[173] I.A. Ibrahheem, M. Koch, Coplanar waveguide metamaterials: the role of bandwidth modifying slots, Appl. Phys. Lett. 91 (2007) 113517.
[174] M. Quinten, A. Leitner, J.R. Krenn, F.R. Aussenegg, Electromagnetic energy transport via linear chains of silver nanoparticles, Opt. Lett. 23 (17) (1998) 1331–1333.
[175] S.A. Tretyakov, A.J. Viitanen, Line of periodically arranged passive dipole scatterers, Electr. Eng. 82 (6) (2000) 353–361.
[176] M.L. Brongersma, J.W. Hartman, H.A. Atwater, Electromagnetic energy transfer and switching in nanoparticle chain arrays below the diffraction limit, Phys. Rev. B 62 (2000) 16356–16359.
[177] W.H. Weber, G.W. Ford, Propagation of optical excitations by dipolar interactions in metal nanoparticle chains, Phys. Rev. B 70 (2004) 125429.
[178] R.A. Shore, A.D. Yaghjian, Traveling electromagnetic waves on linear periodic arrays of lossless spheres, Electron. Lett. 41 (10) (2005) 578–580.
[179] R.A. Shore, A.D. Yaghjian, Traveling electromagnetic waves on linear periodic arrays of lossless penetrable spheres, IEICE Trans. Commun. E 88-B (6) (2005) 2346–2352.
[180] M. Guasoni, C. De Angelis, Analytical approximations of the dispersion relation of a linear chain of nanoparticles, Opt. Commun. 284 (7) (2011) 1822–1827.